CrystEngComm

Accepted Manuscript

ROYAL SOCIETY OF CHEMISTRY

www.rsc.org/crystengcomm

The Role of Solid-State Nuclear Magnetic Resonance in Crystal Engineering

Yijue Xu, Scott A. Southern, Patrick M. J. Szell, and David L. Bryce*

Department of Chemistry and Biomolecular Sciences

University of Ottawa

Ottawa, Ontario

K1N6N5

Canada

phone 613-562-5800 ext 2018

fax 613-562-5170

email dbryce@uottawa.ca

*author to whom correspondence may be addressed

Abstract

An overview of the role of solid-state nuclear magnetic resonance (SSNMR) spectroscopy in the field of crystal engineering is provided. NMR methodologies often provide insights into the structure and dynamics of solid materials which would otherwise be unavailable by X-ray diffraction. More generally, NMR crystallographic structure solutions or refinement approaches seek to incorporate available data from all sources, including the results of density functional theory calculations and diffraction data. This *Highlight* article discusses the state of the field through a recapitulation of relevant theory and selected applications from the literature. Specific topics covered include NMR structure refinement, polymorph identification and differentiation, non-covalent interactions, and the role of dynamics.

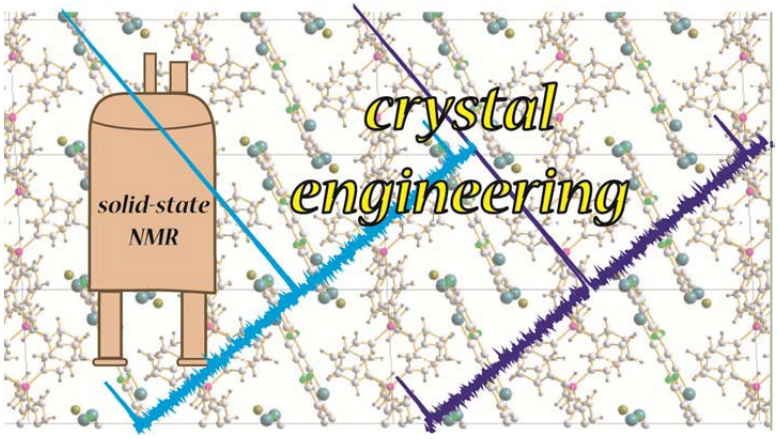

Keywords

Nuclear magnetic resonance, crystallography, halogen bonds, solid-state NMR, non-covalent interactions

1. Introduction

An elementary definition of crystal engineering may be found in the *Scope* of this journal, which is a venue for "innovative research covering all aspects of crystal engineering - the design, including synthesis of crystals and crystal growth, synthesis and evaluation of solid-state materials with desired properties."[1] In the context of the present *Highlight* article, our focus is on the latter part of this scope, with an emphasis on the role of solid-state nuclear magnetic resonance (SSNMR) spectroscopy in the characterization of a range of solid materials and on how the vast repertoire of SSNMR methodologies can be used to advance the field of crystal engineering.

Two of the most commonly used methods for molecular and crystallographic structure characterization are solution NMR spectroscopy and X-ray diffraction (XRD). While these methods clearly continue to be highly successful, they may suffer from limitations in certain cases. First, if one is interested in solid-state structure, dynamics, and properties, solution NMR spectroscopic methods are clearly not relevant. In the case of single-crystal XRD, one may encounter problems with crystallization, crystal size, or solubility, particularly for membrane proteins or other biological systems. It is also well-known that routine XRD refinements do not typically provide highly accurate hydrogen atom positions, but rather use a model based on the locations of the heavy atoms. In order to obtain a proper understanding and interpretation of non-covalent interactions of particular importance to crystal engineering, such as hydrogen bonding, the exact locations of these hydrogen atoms should be determined. Furthermore, motion and disorder of guest molecules in host materials can also be problematic for diffraction techniques. Under these circumstances, SSNMR has proven to be an advantageous complementary or alternative approach in several appealing respects. For instance, it is not

limited to crystalline samples; indeed, glasses and other amorphous or disordered systems are routinely characterized via multinuclear solid-state magnetic resonance methods. This capability arises from the nuclear site-specific nature of NMR techniques. In addition, SSNMR methods have the capacity to provide detailed insight into the nature and timescale of molecular dynamics in solids. Therefore, it is often desirable to combine other solid-state spectroscopic techniques and apply powder XRD in order to obtain valuable complementary information on the structure and properties of powdered microcrystalline materials.

The term 'NMR crystallography' refers to a range of approaches to select, solve, or refine a crystal structure, with a focus on solid-state NMR data. This is typically done in concert with additional data, such as that available from density functional theory (DFT) or *ab initio* calculations, and X-ray diffraction methods, when they are available.[2] Such an approach has proven to be particularly valuable in the cases where diffraction-based methods are not able to provide a complete high-resolution structural model. X-ray crystallography may be limited to providing the unit cell and/or space group, or the result of a Rietveld refinement may simply not be precise enough for the application at hand. The NMR crystallographic approach may be as straightforward as providing specific structural constraints, such as internuclear distances, or sophisticated enough to provide a high-quality complete structural model (*vide infra*).

The role of SSNMR in crystal engineering goes beyond the more limited framework of NMR crystallography. The definition presented by Desiraju, that, "crystal engineering is the understanding of intermolecular interactions in the context of crystal packing and the utilization of such understanding in design of new solids with desired physical and chemical properties,"[3] implies that SSNMR must ultimately contribute to the design and construction of new materials with specific properties. Crystal engineering consists of first describing the solid-state structure,

and then attributing the physical properties of the obtained material to the structure. Once this has been determined, an improved material, obtained either by a modified synthetic procedure or a topotactic transition, for example, can yield a desired property. As such, the accurate characterization of the solid-state structure must be obtained, as any uncertainties, including polymorphism, can play a pivotal role in achieving the engineering objectives. This *Highlight* article presents various vignettes which demonstrate how solid-state NMR spectroscopy is proving to be a powerful tool in the field of crystal engineering. After a brief overview of some of basic information on SSNMR spectroscopic methods, several applications are discussed, with particular emphasis on polymorphism, the role of non-covalent interactions, structure refinement procedures, dynamics, and porous materials.

2. Solid-State NMR Interactions and Fundamentals

In this section, we provide a brief overview of the NMR interactions of relevance to NMR crystallography and crystal engineering applications. Further details on the fundamentals of SSNMR spectroscopy and NMR crystallography may be found in various reviews and books.[2,4,5] The four most common NMR interactions which are relevant to the applications discussed later in this work are (i) magnetic shielding, which leads to the well-known chemical shifts; (ii) direct dipolar coupling, which under favourable circumstances can provide internuclear distances; (iii) electron-mediated *J* coupling between nuclear spins; and (iv) nuclear electric quadrupolar coupling. A fifth section provides a short overview of the fundamentals of SSNMR methodology.

(i) Chemical shifts and chemical shift anisotropy (CSA)

The magnetic shielding (σ) interaction gives rise to the chemical shifts (δ) observed in solution NMR and solid-state NMR. The frequency of a shielded peak is given by:

$$\nu = (1 - \boldsymbol{\sigma})\frac{\gamma B_0}{2\pi} \qquad [1]$$

where $\boldsymbol{\sigma}$ is the second-rank magnetic shielding tensor, γ is the magnetogyric ratio of the nucleus, and B_0 is the applied magnetic field strength. The corresponding chemical shift tensor ($\boldsymbol{\delta} = (\boldsymbol{\sigma}_{ref} - \boldsymbol{\sigma})/(\mathbf{1} - \boldsymbol{\sigma}_{ref})$) may be expressed in Cartesian form as follows:

$$\boldsymbol{\delta} = \begin{bmatrix} \delta_{xx} & \delta_{xy} & \delta_{xz} \\ \delta_{yx} & \delta_{yy} & \delta_{yz} \\ \delta_{zx} & \delta_{zy} & \delta_{zz} \end{bmatrix} \qquad [2]$$

Diagonalization of this tensor provides three principal components, $\delta_{11} \geq \delta_{22} \geq \delta_{33}$, as well as the orientation of the principal axis system in the frame of reference. The magnitude of the tensor is typically re-expressed as a sum of isotropic and anisotropic parts (we ignore the antisymmetric part here). The isotropic chemical shift is simply

$$\delta_{iso} = (\tfrac{1}{3})(\delta_{11} + \delta_{22} + \delta_{33}) \qquad [3]$$

and the anisotropic part is often expressed according to one of two conventions. The first refers to the span (Ω) and skew (κ) of the tensor, and the second refers to an anisotropy parameter (δ_{aniso}) and an asymmetry parameter (η_δ) (note, $|\delta_{zz} - \delta_{iso}| \geq |\delta_{xx} - \delta_{iso}|\ |\delta_{yy} - \delta_{iso}|$).

$$\Omega = \delta_{11} - \delta_{33} \qquad [4]$$

$$\kappa = 3\frac{\delta_{22} - \delta_{iso}}{\Omega} \qquad [5]$$

$$\delta_{aniso} = \delta_{zz} - \frac{\delta_{xx} + \delta_{yy}}{2} \qquad [6]$$

$$\eta_\delta = \frac{\delta_{yy} - \delta_{xx}}{\delta_{zz} - \delta_{iso}} \qquad [7]$$

In addition to the well-known empirical relationships between δ_{iso} and functional group for nuclides such as ^{1}H and ^{13}C, the chemical shift tensor provides much information of relevance to the solid-state structure and crystal packing interactions. In the solid state, each atom will in principle exhibit a different chemical shift unless they are strictly crystallographically equivalent (i.e., related by a symmetry element). This can be particularly valuable in determining or validating a crystal structure solution (e.g., number of molecules in the asymmetric unit, correct space group, correct polymorph).[6] The anisotropy of the chemical shift tensor provides information on the local electronic environment and local symmetry about the atom in question.

(ii) Direct Dipolar Coupling

Direct coupling between the magnetic dipoles of nuclei depends on the motionally-averaged inverse cube of the internuclear distance. This is quantified by the dipolar coupling constant, R_{DD}:

$$R_{DD} = \left(\frac{\mu_0}{4\pi}\right)\left(\frac{\gamma_1\gamma_2\hbar}{2\pi}\right)\langle r_{1,2}^{-3}\rangle \qquad [8]$$

Many standard high-resolution SSNMR methods remove the direct effects of dipolar coupling in order to increase spectral resolution. However, there is a range of methods available to re-introduce the dipolar coupling between selected pairs of spins under high-resolution conditions so that internuclear distances may be determined. Spectra of stationary powdered samples also yield information on the dipolar coupling under favourable conditions. However, one must be cautious in the interpretation of data acquired from a multispin system, which is subject to many simultaneous pairwise dipolar coupling interactions. As shown in eq. 8, the measured dipolar coupling constant reflects the motionally-averaged inverse cube of the

internuclear distance. This can be a hindrance or an advantage: if one has reason to believe there is negligible motion, true internuclear distances can be measured with NMR; on the other hand, if one already has a good estimate of the expected internuclear distance, the difference between the measured and predicted dipolar coupling constant provides proof of dynamics in the system. A final caveat concerns the anisotropic part of the indirect nuclear spin-spin (J) coupling tensor, ΔJ (vide infra). In reality one can only measure an effective dipolar coupling constant, R_{eff}, equal to R_{DD}- $\Delta J/3$. While ΔJ is often negligible for couplings to light elements like hydrogen, it can actually dominate R_{eff} for some heavy elements, thereby complicating the process of translating measured dipolar coupling constants directly into accurate distances. The reader is referred to the recent highlight article by Chierotti and Gobetto on the use of dipolar interactions in polymorph and cocrystal investigations.[7]

(iii) Indirect Nuclear Spin-Spin (J) Coupling

J couplings, familiar from solution NMR spectroscopy, are electron-mediated couplings between nuclear spins. Such couplings can provide valuable information on molecular connectivity and conformation. These couplings have often been referred to as 'scalar' couplings and 'through-bond' couplings, although neither of these terms is entirely apposite. J coupling is properly described by a second-rank tensor, analogous to that presented in equation 2 for chemical shifts. However, in solution and in most cases in the solid state, only the isotropic coupling constant (J_{iso}, a scalar) is normally observed and interpreted. Further information on the tensor properties of J coupling may be found in reference 8.

J couplings measured from spectral splittings may be generally interpreted in a manner analogous to what is routinely done in solution NMR analyses. In the solid state, however, such

spectral splittings may often be obscured by other effects which can broaden in the NMR resonances. Such effects may be attributed to other NMR interactions such as quadrupolar or dipolar broadening, or may be due to the nature of the sample itself. For example, amorphous samples generally give rise to broader NMR lines than do highly crystalline samples.

Recent work by Ashbrook has emphasized another important application of *J* couplings in the solid state.[9,10] It has been demonstrated that *J* couplings between nuclear spins can be observed under favourable conditions in the absence of a covalent bond (or reasonably short bond path) between the two atoms. This implies that *J* couplings can probe weak non-covalent interactions, and such interactions have even been termed 'through-space' *J* couplings. Another interesting application of such couplings in the field of crystal engineering is the potential to observe *J* couplings between adjacent molecules in a crystal. Perras and Bryce have also recently shown how *J* couplings between quadrupolar nuclei can differentiate between equivalent and non-equivalent spin pairs, thereby providing a novel probe of crystallographic symmetry.[11,12,13]

(iv) Nuclear Electric Quadrupolar Coupling

Over two thirds of the NMR-active nuclides in the periodic table are quadrupolar, meaning that their nuclear spin quantum number (*I*) is greater than ½. The interaction between the nuclear electric quadrupole moment (*Q*) of such a nucleus with the electric field gradient (EFG) at the nucleus is called the quadrupolar interaction, and its magnitude is defined using the quadrupolar coupling constant (C_Q) and asymmetry parameter (η_Q):

$$C_Q = eV_{33}Q/h \qquad [9]$$

$$\eta_Q = (V_{11}-V_{22})/V_{33} \qquad [10]$$

where $|V_{11}| \leq |V_{22}| \leq |V_{33}|$ are the principal components of the EFG tensor.

The quadrupolar interaction can cause rapid nuclear spin relaxation, and in solution this may lead to broad NMR lines. Indeed, for nuclei subject to large quadrupolar interactions it can be impractical or impossible to record their resonances in solution. In the solid state, the quadrupolar interaction can lead to broad powder pattern line shapes which may be analyzed to provide information on the local nuclear environment, such as the local symmetry. Quadrupolar coupling data may be analyzed and used in structure refinement protocols in conjunction with X-ray and computational data.[14,15]

(v) Common Experimental Techniques

Typical SSNMR experimental methods are described in various sources.[4,5,16,17] This purposely brief section presents some of the most common techniques employed at a basic level in order to appreciate the discussion of various applications (*vide infra*). The discussion applies to powdered samples.

SSNMR is almost always carried out on powdered samples, although there are also experiments to look at single crystals and other aligned samples.[5,18,19] A 'powdered' sample is most often described as being microcrystalline; however, the particle size may be smaller and indeed as mentioned the 'powder' does not have to be crystalline at all. Sample preparation is important inasmuch as one should think about such questions as: Is the sample dry or solvated? Has the sample been recrystallized from an appropriate solvent? Is the sample homogeneous? For biomolecules in particular, sample preparation is extremely important to achieve relevant results. Crystalline, well-ordered, well-prepared samples will yield spectra with better resolution than will amorphous, disordered, or inhomogeneous samples.

High-resolution SSNMR spectra are typically acquired using magic-angle spinning (MAS). Rapid spinning (~10 to 100 kHz) of a sample about an axis oriented at 54.74° with respect to the applied magnetic field removes or reduces a good number of the anisotropies which contribute to broad SSNMR spectra under stationary conditions. For spin-1/2 nuclei like ^{13}C, ^{15}N, and ^{31}P, the first two of which have low natural abundance, MAS is often combined with cross-polarization (CP) from nearby abundant ^{1}H nuclei, resulting in an increase in the sensitivity of the observed nucleus. Under appropriate conditions, CP/MAS SSNMR spectra of spin-1/2 isotopes often provide 'solution-like' spectra consisting of sharp peaks, the positions of which are described by the isotropic chemical shift, δ_{iso}. If the spinning is not sufficiently fast, or the CSA is large relative to the spinning rate, then each true peak is flanked by spinning sidebands at integer multiples of the spinning rate (see Figure 1). Methods are available to suppress the spinning sidebands, such as the 'total suppression of spinning sidebands' (TOSS) pulse sequence.[20] *J* couplings may also affect the spectra in a manner analogous to what is observed in solution NMR spectroscopy. The resonances of spin-1/2 nuclei which are directly bonded to other spin-active isotopes may show additional broadenings due to residual dipolar couplings; these can be valuable in providing structural information.

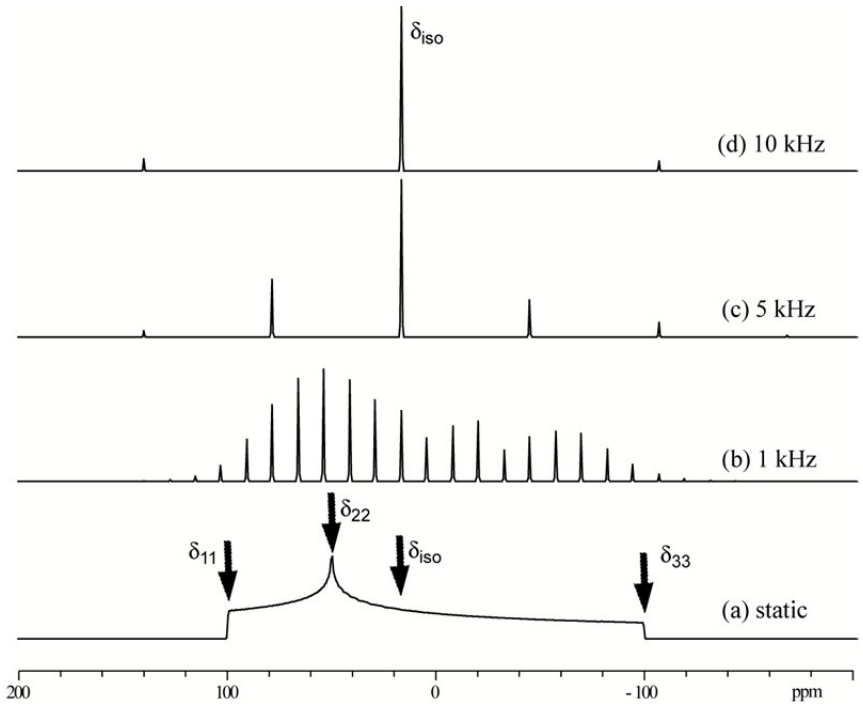

Figure 1. Simulated solid-state NMR spectra for an isolated spin-1/2 nucleus in a powdered sample. (a) Shows a powder pattern for a stationary sample, with discontinuities corresponding to the principal components of the chemical shift tensor indicated, as well as the isotropic chemical shift. Shown in (b), (c), and (d) are magic-angle spinning spectra for various rotor speeds. The isotropic chemical shift does not change frequency from one spectrum to the next. Conversely, the spinning sidebands (to high and low frequency of the centreband (δ_{iso})) move and change intensity with the spinning speed.

For the 99.6% naturally abundant ^{1}H isotope, strong homonuclear dipolar coupling interactions typically dominate the SSNMR spectrum. Combined rotation and multiple pulse (CRAMPS) experiments, or simply very fast MAS, are employed to achieve high-resolution spectra. DUMBO is a popular radiofrequency pulse scheme used for this purpose.[21] Even with such sophisticated experiments, the resolution of ^{1}H SSNMR spectra is less than that available from solution ^{1}H NMR experiments.

The SSNMR spectra of quadrupolar nuclei are broadened by the nuclear electric quadrupolar interaction, in addition to the broadenings due to CSA and internuclear couplings. The spectra, even under fast MAS conditions, therefore feature an anisotropic residual second-order broadening. These broad line shapes are valuable however, as they may be fit using

analytical software to determine the quadrupolar coupling constant and asymmetry parameter. Higher resolution may be achieved for half-integer spin quadrupolar nuclei using methods such as multiple-quantum magic angle spinning (MQMAS), satellite transition MAS, double-rotation, or dynamic angle rotation. The reader is referred to references 22, 23, 24, and 25 for further information on these methods.

3. Applications

This section highlights particular literature reports which have been chosen to provide a sense of the field in general and of the breadth of applications. This section is divided into the following categories to provide some perspective on the field, and for ease of reading; however, clearly some reports may fit into multiple areas: (i) fingerprinting and polymorphism; (ii) non-covalent interactions; (iii) structure refinement; (iv) dynamics and porous materials.

(i) Spectral Fingerprinting and Polymorphism

An NMR-active nucleus of each crystallographically distinct atom in the asymmetric unit will give rise to a different chemical shift, although fortuitous overlap is always possible. Thus, the solid-state NMR spectrum will be diagnostic not only of the chemical (molecular) structure as is the solution NMR spectrum, but it will also be sensitive to the crystallographic structure and symmetry. For example, the spectrum will often clearly provide the number of molecules in the asymmetric unit (Z').[6] The tensor properties of the chemical shift and the other NMR properties described above will also be exquisitely sensitive to the solid state structure, including important features such as non-covalent interactions between adjacent molecules and the space group symmetry. The solid-state NMR spectrum of a given sample is therefore diagnostic of both the

chemical and the crystallographic structure. This uniqueness is reminiscent of the 'fingerprint' obtained from a powder X-ray diffractogram. ^{13}C chemical shifts for well-behaved crystalline compounds are easily reproducible to within ~0.1 ppm under appropriate conditions. ^{13}C chemical shifts may only be reliable to the nearest ~1 ppm or so in other cases, e.g., for some amorphous materials or for spectra with low signal-to-noise ratios.[26,27,28]

For example, Bardelang *et al*. applied ^{13}C CP/MAS SSNMR spectroscopy to several cucurbituril materials.[29] The chemical shift and splitting pattern of the three chemically distinct carbon functionalities, CH_2, C=O, and CH, can serve as a spectroscopic fingerprint for such materials. Also, since there is a correspondence between the ^{13}C resonances and the number of unique carbon sites from known crystal structures, any additional ^{13}C NMR peaks in different samples may serve as an indication of a potential new phase of unknown structure.

In another example, a set of three supramolecular compounds with different hydrogen bonding motifs, *N*,*N'*-(cyclohexane-*trans*-1,4-diyl)bis(2,2-dimethylpropanamide) (**1**), 1,1'-(cyclohexane-*trans*-1,4-diyl)bis(3-*tert*-butylurea) (**2**) and N^1,N^4-bis(*tert*-butylcarbamoyl)cyclohexane-*trans*-1,4-dicarboxamide (**3**) were found to form only crystalline powders, preventing single crystal X-ray diffraction analysis. All signals in the ^1H DUMBO, ^{13}C CP/MAS and ^{15}N CP/MAS spectra were assigned with the help of ^1H-^{13}C and ^1H-^{15}N 2D HETCOR experiments. The favoured spatial proximities of NH protons and possible hydrogen bonding patterns were obtained from ^1H-^1H double-quantum/single-quantum correlation experiments for compounds **2** and **3**. A combination of symmetry information from one-dimensional ^{15}N and ^{13}C NMR spectra and indexing of the powder pattern limited the possible space groups of compound **1** and **2** to be $P2_1/c$, and compound **3** to be $P\bar{1}$.[30]

Polymorphism is the ability of a compound to exist in more than one crystal form, which generally leads to a change in its physical properties, such as melting point, solubility and thermodynamic processes etc.[31] There are several concerns with respect to conformational variability, solubility, and dissolution rate in drug design; therefore, the potential of polymorphism can play a significant role in pharmaceutical research and development. A well-known example of pharmaceutical polymorphism causing real-world problems is that of ritonavir (a protease inhibitor for HIV); some samples failed dissolution tests because of the existence of another crystal form (Form II).[32] Typical analytical techniques that are used for characterization or identification of polymorphs include infrared spectroscopy, Raman spectroscopy, scanning electron microscopy, X-ray crystallography and solid-state NMR.[31]

Enright et al. carried out ^{13}C CP/MAS SSNMR experiments on anhydrous polymorphs of caffeine, the results of which enabled an improved description of the proper space groups and structures when combined with additional X-ray diffraction experiments.[33] Indeed, these NMR results allowed for the correction of the erroneous space group which had been previously proposed on the basis of powder XRD alone. The ^{13}C CP/MAS spectra of various forms of caffeine shown in Figure 2 nicely demonstrates the clear-cut capabilities of this method in differentiating between polymorphs as well as hydrates.

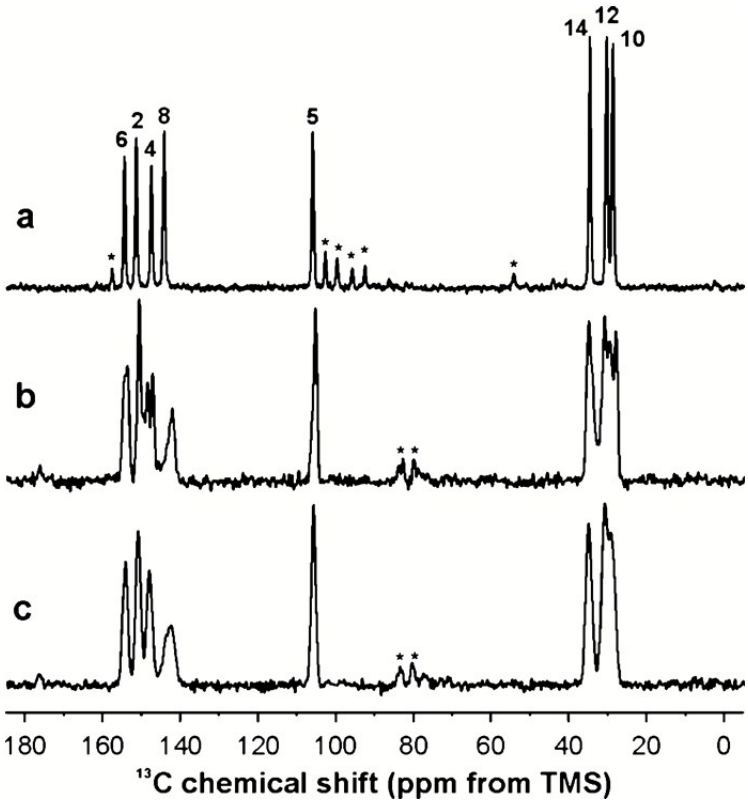

Figure 2. ^{13}C CP/MAS NMR spectra of three forms of caffeine recorded at a Larmor frequency of 226.3 MHz: (a) monohydrate; (b) low-temperature anhydrous form; (c) high-temperature anhydrous form. The asterisks indicate spinning sidebands. Copyright 2007 American Chemical Society. Used with permission. From reference 33.

Veinberg *et al.* used ultra-wideline ^{14}N solid-state NMR to differentiate three polymorphic forms of glycine and an HCl salt derivative.[34] Nitrogen-14 is a spin-1 nuclide which typically gives rise to very broad NMR line shapes in powders. This can pose technical challenges as described in ref. 34 (and references therein), but the method nevertheless can provide valuable information. Three different polymorphs of glycine (α, β, γ) have slightly different ^{14}N quadrupolar parameters. In particular, distinct η_Q values are characteristic of different locations of "horn", "shoulder" and "feet" discontinuities in the spectra. The effective transverse relaxation time constants $T_2^{\text{eff}}(^{14}\text{N})$ were also found to be different for all polymorphs.

β–glycine has shortest $T_2^{eff}(^{14}N)$ value due to heteronuclear ^{14}N-^{1}H dipolar coupling. They further carried out variable-temperature ^{14}N NMR experiments on α- and γ-glycine, as well as the HCl salt derivative, to calculate the correlation time τ_c characteristic of the motion of NH_3 group in the molecule.

Hildebrand *et al*. applied ^{35}Cl solid-state NMR to a series of HCl salts of active pharmaceutical ingredients for spectral fingerprinting and polymorph recognition.[35] They examined two systems: isoxsuprine HCl (Isox) and mexiletine HCl. IsoxI is a polymorph of Isox which was recrystallized from methanol. Unlike Isox, which has only one chlorine site involved in four short hydrogen contacts in the asymmetric unit, IsoxI has two distinct chlorine sites which are both involved in four short hydrogen contacts. These sites give rise to overlapping powder patterns in the static ^{35}Cl SSNMR spectra at 9.4 T. One crystallographic chlorine site in each of IsoxI and Isox have similar quadrupolar tensor magnitudes and orientations, but different CS tensor parameters. ^{1}H-^{13}C variable-amplitude cross-polarization (VACP) MAS spectra of Isox and Isoxl differed in the aromatic region, which can be used to fingerprint the two polymorphs. This work demonstrates nicely the role of ^{35}Cl and ^{13}C SSNMR in differentiating between polymorphic forms of pharmaceuticals.

SSNMR fingerprinting in combination with X-ray methods has also helped in the assignment of space groups to unknown polymorphs of certain materials. Burgess *et al.* presented a systemic analysis of the vaterite polymorph of $CaCO_3$ by a combination of PXRD, ^{43}Ca SSNMR experiments, and computations.[36] Simulated PXRD patterns from proposed vaterite crystal structures were compared to experimental PXRD data to rule out some models which have inconsistent PXRD data (such as monoclinic $C\bar{1}$, $C2/c$ as well as DFT predicted

GGA, LDA and $P2_12_12_1$). Experimental ^{43}Ca chemical shifts from DOR NMR and $|C_Q(^{43}Ca)|$ values from ^{43}Ca MAS NMR spectra were compared with values from GIPAW (Gauge-Including Projector-Augmented Wave) DFT calculations generated using the various proposed vaterite structures. Additional models were thus ruled out due to large differences between the experimental values and calculated values (i.e., the orthorhombic *Ama*2 and *Pbnm* and the hexagonal $P6_3/mmc$ models). Finally, they found the $P3_221$ model and monoclinic *C*2 model to be most consistent with both the PXRD pattern as well as experimental and calculated ^{43}Ca NMR parameters.

Wang *et al.* used SSNMR to discriminate between the two forms (keto and enol) of acesulfame (AH) in a pharmaceutical cocrystal with theophylline (THP).[37] By ethanol-assisted grinding with a starting THP/AH ratio of 1:2, a novel pharmaceutical cocrystal (THPAH12) was obtained. ^{13}C CP/MAS TOSS NMR spectra, as well as ^{15}N CP/MAS NMR spectra, were used to analyze THPAH12, THP, and AH. Remarkable differences were noted in the chemical shifts of carbons C8/C8', C9/C9' and C10/C10', implying differences in the conformations of each of the AH molecules. Furthermore, the change in the position of the C9 signal implied the change of one of the AH molecules to the tautomeric (AH enol) or ionized (AH^-) state in the 1:2 cocrystal.

SSNMR methods can be used to discern between the various temperature-dependant phases of certain materials. Smet *et al.* looked into the solid–state phase transitions between the α, β and γ forms of DL-norleucine using variable-temperature ^{13}C CP/MAS.[38] They were able to observe $\alpha \leftrightarrow \beta$ (at 138 K) and $\alpha \leftrightarrow \gamma$ transitions (at 393 K). A large change in the N1-C2-C3-C4 torsional angle as a result of the $\alpha \leftrightarrow \gamma$ transition led to a relatively large difference in the chemical shifts of C3 to C6 of the carbon chain. By comparing variable-temperature ^{13}C CP/MAS spectra for powder samples and single crystals, they found out that $\alpha \leftrightarrow \beta$ transition is

faster in a single crystal than in the powder sample, and that these two polymorphs can coexist in the single crystal over a large temperature range.

In addition to polymorphism, crystal structures may also change depending on their hydration or solvation state. The resulting materials are referred to as hydrates, solvates, or sometimes pseudopolymorphs. An example is the Tyr-$_D$-Ala-Phe-Gly (YAFG) peptide fragment. NMR spectroscopy has also been employed to characterize the hydrated form of this tetrapeptide, as well as to characterize the unknown structure of its dehydrated form. By applying both homonuclear (^{13}C-^{13}C SHANGHAI, ^{1}H-^{1}H BABA) and heteronuclear 2D correlations (^{1}H-^{13}C and ^{1}H-^{15}N) with inverse detection), Pawlak *et al*. were able to make the spectral assignments of all of the carbon and proton positions in both forms. The results suggest that the pseudo-cyclic structure of the peptide was preserved upon its dehydration. Furthermore, after geometry optimization, GIPAW DFT was used calculate the ^{13}C chemical shift tensors and ^{1}H isotropic chemical shifts. The reconstruction of the peptide crystal structure from the collected data of the dehydrated YAFG peptide yielded a final proposed structure.[39]

NMR spectroscopy has been used extensively to confirm or fingerprint the crystal structures of pharmaceutical compounds. A series of sodium naproxen hydrates has been characterized by means of ^{23}Na SSNMR by Burgess et al.[40] Significant changes in the ^{23}Na quadrupolar interaction were observed for each hydrated state as a result of the different oxygen coordination environment resulting from the water molecules. The reported ^{23}Na quadrupolar coupling constant for the anhydrous form of sodium naproxen was of 2.88(0.03) MHz for the first site, and 3.08(0.03) MHz for the second site. In contrast, the monohydrated form had a C_Q value of 1.08(0.03) MHz, and the methanol solvate had a C_Q of 3.05(0.02) MHz. Experiments using double rotation NMR (DOR) to average the first and second order quadrupolar interaction,

yielded solution-like spectra and revealed the multiple hydrated forms in commercial sodium naproxen (Figure 3). Bond et al. provided additional valuable insights from ^{13}C and ^{23}Na SSNMR into the disorder in the structure of the sodium naproxen tetrahydrate. [41] Two resonances seen for the naproxen methyl group in ^{13}C CP/MAS SSNMR spectrum are accounted for by the presence of two orientations along the doubled *b* axis for the carboxyl group. A single resonance in the ^{23}Na SSNMR was found to be consistent with local $2_1/m$ symmetry in the Na^+/H_2O regions of the compound. This work illustrates how SSNMR can be a useful tool in determining fine structural details of compounds exhibiting disorder.

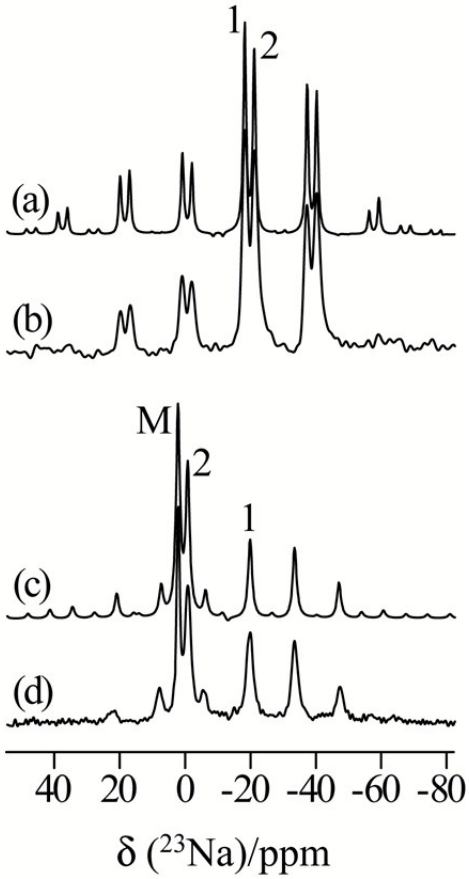

Figure 3. ^{23}Na DOR solid-state NMR spectra of solvates of sodium naproxen. Both anhydrous (b) and the methanol solvate (d) of sodium naproxen were acquired at B_0 = 9.4 T. Numbers indicate the peak corresponding to each site. Density matrix simulations (a and c) were

performed in order to accurately simulate the experimental spectra. Copyright Elsevier 2012. Used with permission. From reference 40.

Apperley and co-workers applied SSNMR to characterize the structure of solvates and polymorphs of formoterol fumarate.[42] With the help of solution NMR, dipolar dephasing experiments, and GIPAW DFT computations, ^{13}C resonances were assigned to the crystal structures of diethanol and diisopropanol solvates of formoterol fumarate. Polymorphs 'A' and 'C', the detailed structures of which are not available, were also prepared and ^{13}C spectral assignments were carried out where possible. HETCOR and fast-MAS ^{1}H experiments performed on the diethanolate form and polymorph C provided information on the hydrogen bonds in these systems, with form C showing stronger hydrogen bonding than the solvates. Phenylene ring flips were studied by ^{13}C CP/MAS, and it was concluded that the rotation barrier is lower in the solvates than in form C. Additional ^{13}C and ^{2}H relaxation experiments suggested that the fumarate ion undergoes small-amplitude motion in the desolvate.

Chandrappa *et al.* identified three polymorphs of xaliproden: Form II is orthorhombic and Form I and III are monoclinic.[43] Slight differences between Form I and III were identified by high-resolution synchrotron powder XRD. To understand the structural disorder in Form III, X-^{13}C (X = ^{1}H or ^{19}F) CP/MAS NMR spectra were recorded under either ^{1}H or $^{1}H/^{19}F$ decoupling conditions. The results showed ^{19}F self-decoupling in Form III and allowed the authors to conclude that the structural disorder observed is of dynamic origin (*i.e.*, rotation of the CF_3 group around the carbon-carbon single bond). This valuable study shows that the polymorphism of xaliproden Form I and Form III is mainly associated with the motion of the CF_3 group, rather than any major static structural differences.

Structural features of a series of Group 13 ion binary and ternary species of benzilic acid and phenanthroline ($[B(C_{14}H_{10}O_3)_2](C_3H_5N_2)\cdot H_2O$ (**4**), $[Al(C_{14}H_{11}O_3)_3]\cdot 0.5C_2H_5OH\cdot 4.5H_2O$ (**5**), $[Ga(C_{14}H_{11}O_3)_3]\cdot CH_3OH\cdot 3H_2O$ (**6**), $[In(C_{14}H_{11}O_3)_4]\cdot C_3H_5N_2\cdot C_2H_5OH\cdot H_2O$ (**7**), $[Tl(C_{14}H_{11}O_3)_4]_n$ (**8**) , $[Tl_2(C_{14}H_{11}O_3)_2(phen)_2]$ (**9**), $[Tl(C_{14}H_{11}O_3)(phen)(H_2O)](C_{14}H_{12}O_3)(phen)$ (**10**)) have been determined using multinuclear (^{13}C, ^{11}B, ^{27}Al, ^{71}Ga, and ^{205}Tl) magnetic resonance.[44] RAMP CP/MAS ^{13}C NMR was applied to all seven molecules to show the unique resonances associated with different ligand binding modes. ^{11}B, ^{27}Al, and ^{71}Ga MAS NMR reflect the mononuclear nature of compounds **4**, **5**, and **6**. An unstructured ^{205}Tl broad line shape differentiates the structure of **8** from other coordinated Tl materials. This study shows the value of a multinuclear approach to gaining insight into such structural features as coordination mode.

More recently, Hammann *et al*. applied ^{71}Ga NMR to characterize the structure and coordination environments of several heterometallic Group 13 hydroxoaquo clusters, $[Ga_{13-x}In_x(\mu_3\text{-}OH)_6(\mu_2\text{-}OH)_{18}(H_2O)_{24}]^{15+}$.[45] These clusters, which serve as thin film transistor precursors, share a common motif consisting of one gallium atom at the center ("core"), connected to gallium atoms ("middle ring") by μ_3-OH bridges, then connected to six-coordinate metal sites ("outer ring") *via* μ_2-OH bridges. They first studied Ga_7In_6 and Ga_{13}, two more ordered compounds. Ga_{13} served as a guide to assign NMR parameters to the corresponding sites in the $Ga_{13-x}In_x$ heterometallic clusters. The core and middle Ga species were observed in Ga_7In_6, but the outer Ga site seen in Ga_{13} is absent in Ga_7In_6, which is consistent with the identity of six-coordinate Ga found in single-crystal X-ray structures. They also applied similar methods to heterometallic $Ga_{13-x}In_x$ clusters with disordered structures. The core Ga site always gives a narrow NMR line shape. The C_Q value increases as a result of the indium incorporation, indicating that the core site has a larger distortion. The outer Ga sites are well defined in Ga_{13},

$Ga_{12}In_1$, and $Ga_{11}In_2$. They are similar with a slight increasing trend in C_Q with incorporation of In. The outer ring is absent in Ga_7In_6. Ga_8In_5 might have a too broad lone outer ring gallium to be observed in NMR spectra. The large C_Q values of the middle Ga sites make the line shapes too broad to be resolved well. The η_Q value approaches zero with the incorporation of In. They also performed a longitudinal strain analysis to observe the relationship between quadrupolar coupling parameters and the distortion of octahedral sites. They found that there was a linear correlation between the C_Q values and Ga-O bond length distortion.

(ii) Non-Covalent Interactions

Inter- and intra-molecular non-covalent interactions are an essential part of the crystal engineering toolbox used to influence the crystal structure. In this context, SSNMR is a valuable and complementary tool often used with other methods, such as XRD, for characterizing various non-covalent interactions. These include, for example, hydrogen bonding, π-stacking, and halogen bonding. Halogen bonds are part of a broader class of interactions known as σ-hole interactions,[46] and these have also begun to be explored by SSNMR methods. The presence or absence of non-covalent interactions typically has some effect on one or more of the NMR observables (e.g., chemical shifts, quadrupolar couplings, J couplings). These effects can either be used in a qualitative sense to confirm the presence of a non-covalent interaction, or ideally can be used quantitatively to garner precise geometrical or structural information. SSNMR methods have contributed significantly to the investigation and understanding of non-covalent interactions in solids. Below, selected examples related to a few classes of non-covalent interactions are discussed.

(a) Hydrogen Bonding

Hydrogen bonds are a very important and widely used tool in crystal engineering. They also play critical roles in the structure and function of a variety of biochemical systems such as proteins and nucleic acids. NMR spectroscopy has historically played an important role in the characterization of hydrogen-bonded systems, first in solution, and more recently in the solid state. Consider for example the well-known increases in ^{1}H chemical shifts associated with hydrogen bonds in some systems in solution. In the solid state, ^{1}H NMR spectra long suffered from low resolution due to dominant homonuclear dipolar couplings which are notoriously difficult to completely remove through standard techniques such as magic angle spinning. Technological advances, including faster spinning and sophisticated radiofrequency pulse sequences, now provide much improved ^{1}H spectral resolution in the solid state, allowing for detailed studies of hydrogen bonding environments in solids. Indirectly detected methods, such as ^{14}N-^{1}H HMQC spectroscopy, have created new opportunities in this area.[47] A variety of other probe nuclei may also be used to study hydrogen bonds (e.g., ^{17}O, ^{15}N, ^{13}C, ^{35}Cl, etc.), directly or indirectly, as described through examples below.

A thorough NMR crystallography approach to studying intermolecular crystal packing by a combination of high-resolution solid-state NMR spectroscopy with GIPAW DFT chemical shift calculations was provided by Webber et al.[48,49] NMR data from ^{1}H-^{13}C HMQC correlation spectra were combined with GIPAW DFT chemical shift calculations on the crystal structure of γ-indomethacin for the complete assignment of the ^{13}C and ^{1}H resonances. A comparison between ^{1}H chemical shifts for the fully packed crystal structures and those for isolated molecules provides insight into intermolecular interactions within the crystal, namely hydrogen bonding and aromatic π-π interactions. ^{1}H-^{1}H double-quantum (DQ) CRAMPS NMR and ^{1}H

(DQ-DUMBO)-^{13}C refocused INEPT NMR were used to further probe the H-H contacts that characterize the crystal packing. They examined the ^{1}H DQ integrated intensity curves as a function of the total DQ recoupling time, τ_{rcpl} , for the two DQ peaks at the OH single-quantum resonance, which were further compared to eight-spin density-matrix simulations for a cluster of ^{1}H nuclei corresponding to the OH proton and the seven nearest protons. This provided quantitative information about the intermolecular H-H proximities.

Pogorzelec-Glaser *et al*. provided a description of the hydrogen bonding present in the structures of benzimidazole-glutaric acid and benzimidazole-pimelic acid by a combination of X-ray diffraction, ^{13}C CP/MAS NMR specroscopy, and DFT computations.[50] In a subsequent study, the hydrogen bonding network in benzimidazole-sebacic acid, a proton conductor, was characterized using ^{1}H and ^{13}C MAS NMR, along with DFT calculations.[51] This work also provided insight into the factors which influence hydrogen bonding networks and proton dynamics in crystallized benzimidazole salts by the analysis of proton spin-lattice relaxation time constants, T_1.

Rees *et al.* conducted a combined multinuclear solid-state NMR, X-ray diffraction, and DFT computational study of hydrogen bonding in benzoic acid (BZA) and the full series of the corresponding alkali metal hydrogen dibenzoates (HD).[52] They reported a correlation between the ^{1}H chemical shift and the hydrogen bonding strength, and classified BZA and LiHD as weak hydrogen bonding systems whereas KHD, RbHD**,** and CsHD were found to feature strong hydrogen bonds. The ^{17}O MAS and high-resolution DOR SSNMR experiments provided information on the number of crystallographically distinct oxygen sites in each hydrogen-bonded system. They also showed a good agreement between the experimental and calculated ^{7}Li, ^{39}K, ^{87}Rb, ^{133}Cs NMR parameters; accurate DFT prediction of quadrupole tensor parameters is

consistent with an improved description of the hydrogen bonding arrangement, in particular the precise positions of the hydrogen atoms.

^{17}O SSNMR is a sensitive tool for probing hydrogen bonding in pharmaceutical cocrystals, due to the strong influence of hydrogen bonding on ^{17}O NMR parameters.[53] In a study by Vogt et al., several forms of the anti-inflammatory drug diflunisal were ^{17}O-enriched and studied by ^{17}O MAS NMR.[54] The crystalline Form I, the cocrystal of difunisal with pyrazinamide, and two amorphous dispersions of the drug with polyvinylpyrrolidone (PVP) and hydropropylmethylcellulose acetate (HPMC-AS) were all prepared with an ^{17}O label on both of the carboxylic acid oxygen atoms (O1 (C=O); O2 (C-OH)). The δ_{iso} values extracted from ^{17}O MAS NMR spectra offer a direct view of hydrogen bonding in both the C=O acceptor and the O-H donor; an increase in δ_{iso} of the O2 site by about 7 ppm upon the formation of the diflusinal pyrazinamide cocrystal from Form I implies the presence of a short hydrogen bond. In addition to this, an increase of 12 ppm is observed on the O1 site of the same species, indicating that the C=O participates in a longer H-bond. A further 2D ^{1}H-^{17}O CP-HETCOR spectrum provided additional intra-molecular hydrogen bonding features in the absence of a crystal structure.

Braga *et al.* prepared four lidocaine molecular salts of dicarboxylic acids (oxalic, fumaric, malonic, and succinic) and characterized the presence and the strength of hydrogen bonding by comparing the ^{1}H chemical shifts for hydrogen-bonded proton.[55] Also, 2D ^{1}H-^{1}H DQ CRAMPS and ^{1}H-^{13}C HETCOR confirmed the similarity between the structure of hydrogen-fumarate and hydrogen-succinate (Figure 4). By comparing the structural similarity between the two salts, and using sophisticated SSNMR techniques in combination with PXRD, the structure of hydrogen-succinate was determined.

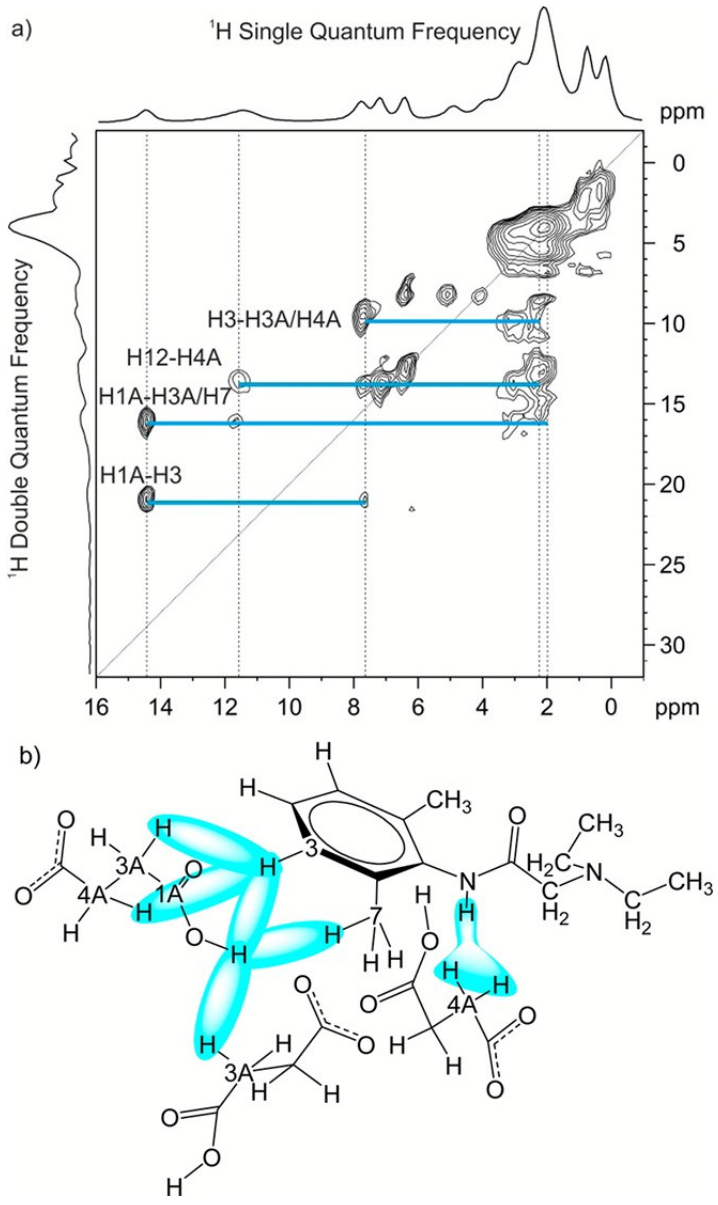

Figure 4. 2D ^{1}H–^{1}H DQ CRAMPS spectrum of hydrogen succinate recorded with a spinning speed of 12.5 kHz. Solid blue horizontal bars indicate specific DQ coherences among H1A, H3, H12, H3A, and H4A. (b) Representation of the crystal structure of hydrogen succinate showing the main ^{1}H–^{1}H intermolecular proximities characterizing crystal packing and HB environments. Copyright American Chemical Society 2013. Used with permission. From reference 55.

In addition to hydrogen bonding with oxygen, it has been found that ^{35}Cl EFG tensors are sensitive to the hydrogen bonding environments of each chloride anions and there are several

notable trends can be observed.[35,56,57] For most single H···Cl contact systems, V_{33} is directed near or along the direction of the shortest contact and the Cl EFG tensors are nearly axially symmetric (η_Q is close to zero). For two H···Cl contacts, either V_{22} or V_{33} is directed near the direction of the shortest contact whereas the other EFG components stay nearly perpendicular to the H-Cl-H plane. In this case, the C_Q values tend to be lower than those in the previous case, and η_Q is higher. For systems with three or more short contacts, no "typical" EFG tensor orientations are observed and the C_Q values were found to be lowest in magnitude in these systems. The sign of C_Q cannot be experimentally determined but can be predicted through theoretical calculations, and it highly depends on ^{35}Cl EFG tensor orientations instead of simply on the number of short H···Cl contacts.

While the NMR parameters of various heteronuclei can be quite sensitive to hydrogen bonding, ^{1}H NMR is also clearly a useful probe of this interaction. Recently, Sardo *et al.* presented the structure of a cocrystal formed by 3,5-dimethyl-1H-pyrazole (dmpz) and 4,5-dimethyl-1H-imidazole (dmim) by powder X-ray diffraction combined with SSNMR.[58] 1D ^{1}H, ^{13}C, ^{15}N as well as 2D ^{1}H-^{13}C (PRESTO and LG-CP) HETCOR and 2D ^{1}H-^{1}H DQ-SQ spectroscopy helped to establish a helical hydrogen-bonded network constructed by two different N-H···N hydrogen bonds formed between one dpmz and two distinct dmim molecules as well as a C-H···π network between all dmim residues. The crystal packing effect was assessed quantitatively by comparison of ^{1}H chemical shifts between solution-state NMR and solid-state NMR.

Jun and co-workers identified six chemically similar but crystallographically non-equivalent hydrogen sites in the α-$Mg_3(HCOO)_6$ metal-organic framework by measuring H-H

proximities using 2D DQ BABA ^{1}H SSNMR.[59] They also looked at different guest-host interactions by observing MAS ^{1}H spectra of deuterated (20% H) samples loaded with a series of different guests: DMF, benzene, and pyridine. Weak C-H···O hydrogen bonding was observed in DMF-loaded samples and C-H···N hydrogen bonding interactions were observed in pyridine-loaded α–$Mg_3(HCOO)_6$, which has no known crystal structure.

(b) Halogen Bonding

σ-hole interactions occur between a localized region of depleted electrostatic potential on a particular atom, and an electron donor. Such interactions are further classified according to the identity of the electron acceptor. Halogen bonds (XB) have risen to prominence in recent years, as is made clear by a recent comprehensive review by Cavallo *et al.*[60] These bonds are of particular interest to the crystal engineering community in part due to their strengths which are in many instances comparable to hydrogen bonds, and due to their predictable linear geometries. A review of SSNMR studies of halogen bonded adducts is available.[61]

Widdifield *et al.* described a multinuclear (^{13}C, ^{14}N, ^{15}N, ^{19}F, and ^{127}I) SSNMR study of a series of halogen-bonded cocrystalline products between decamethonium diiodide and different *para*-dihalogen-substituted benzene moieties.[62] By comparing with NMR data from starting material, they showed that this multinuclear SSNMR experiment could be a very sensitive probe for the formation of the halogen bonding. For example, δ_{iso}(^{13}C) increases in the presence of a halogen bond. C_Q (^{14}N) was found to decrease in the halogen-bonded compounds.

Further to this, a series of halogen (^{35}Cl, ^{81}Br, and ^{127}I) solid-state NMR experiments were applied to characterized the weak halogen bonding present in solid haloanilinium halides.[63] They revealed several notable trends when a series of halogen-bonded compounds are packed in

the same space group. The ^{81}Br isotropic chemical shift and span both decrease as the bromide-halogen XB is weakened, which was supported by accompanying GIPAW DFT calculations on the crystal structures, as well as DFT calculations on isolated models. Following this direct study on halogen bonding donors, an indirect study on cocrystallization of halide salts and *para*-diiodotetrafluorobenzene using zeroth-order regular approximation density functional theory (ZORA-DFT) calculations and ^{13}C SSNMR[64] offered insights into the correlation between the strength of the halogen bond and the δ_{iso} values of the carbon that were covalently bonded to iodine involved in halogen bonding. In addition, a direct investigation of halogen bonding in the solid state using solid-state multinuclear magnetic resonance spectroscopy and molecular orbital analysis provided important insights into the nature of the halogen bond.[65] A series of halogen bonded compounds was synthesised by dissolving equimolar amount of three diiodobenzene derivatives in dichloromethane with an ammonium or phosphonium salt. $^{35/37}$Cl and $^{79/81}$Br SSNMR parameters were correlated to the local XB environment. For example, C_Q(^{35}Cl) values are different in octahedral and square-planar chloride ion coordination systems (Figure 5). A further natural localized molecular orbital (NLMO) analysis revealed that halogen quadrupolar coupling constants and asymmetry parameters correlate with the local halogen bonding geometry of type I···X$^-$···I (X = Br or Cl).

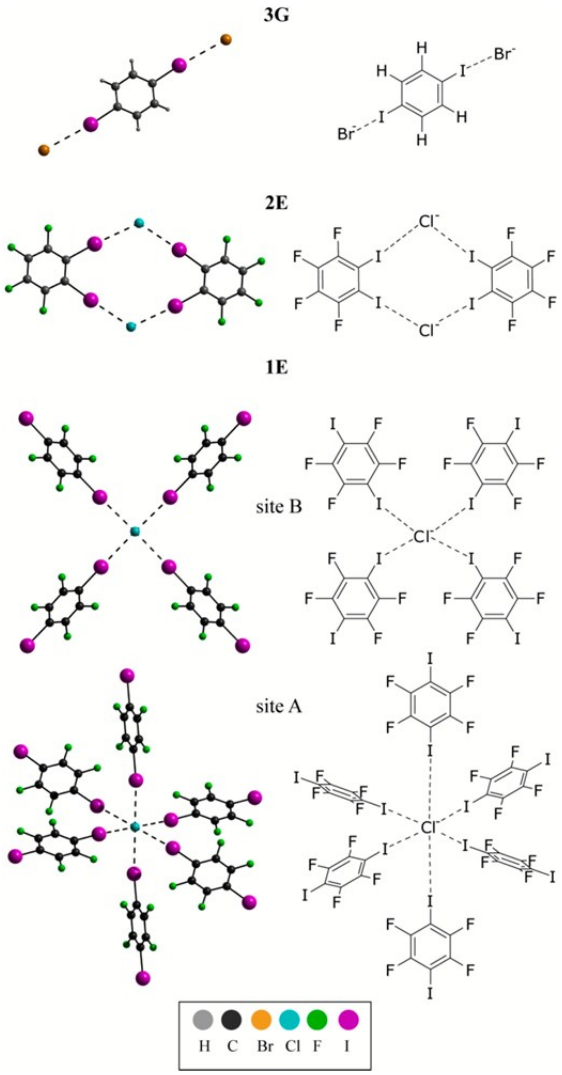

Figure 5. Halogen-bonded structures, from X-ray diffraction (left), and corresponding molecular structure schemes (right). **1E** has two crystallographically distinct chloride sites, where the symmetries about sites A and B are almost perfectly octahedral and square planar, respectively. Cations are not shown. Copyright American Chemical Society 2014. Used with permission. From reference 65.

Several halogen-bonded P=Se···I-C motifs were characterized by X-ray diffraction and multinuclear (^{77}Se, ^{31}P, ^{13}C) SSNMR.[66] ^{77}Se SSNMR indicated an increase in the magnitude of $J(^{31}\text{P}, ^{77}\text{Se})$ and ^{77}Se chemical shift values as the XB weakens. The NLMO DFT approach offered insights into the orbital contribution to the $J(^{31}\text{P}, ^{77}\text{Se})$: The contribution from selenium lone pair orbital, the P=O bonding orbital and the phosphorus core orbital are the three main

factors, and the contribution from the selenium core orbital dominates the linear correlation between the $J(^{31}P, ^{77}Se)$ and halogen bonding.

Most recently, a series of compounds featuring P=O···I-C halogen bonding interaction was prepared by simple mechanochemical acetonitrile-assisted grinding.[67] Nonlabeled and ^{17}O-labelled compounds were characterized by single-crystal X-ray diffraction and solid-state multinuclear (^{31}P, ^{17}O) magnetic resonance at three different applied magnetic field strengths (9.4, 11.7, and 21.1 T). The ^{31}P CS tensors obtained from ^{31}P CP/MAS tend to be sensitive enough to distinguish the halogen-bonded compounds from starting materials. This first study of ^{17}O NMR parameters in halogen-bonded solids provided several correlations between the NMR observables and halogen bonding strength. For example, the ^{17}O quadrupolar coupling constant, asymmetry parameter, and $J(^{31}P, ^{17}O)$ coupling increase in the presence of a halogen bonding interaction. DFT calculations reveal a linear trend between the ^{17}O isotopic chemical shift as well as $J(^{31}P, ^{17}O)$ coupling and halogen bonding strength. An additional NLMO analysis shows an increase in the value of $J(^{31}P, ^{17}O)$ coupling is due to the overall contribution from the P=O bonding orbital, the O lone pair orbital, and the O core orbital. Another NLMO analysis applied to the ^{17}O quadrupolar coupling constant reveals a linear correlation between the oxygen p_z lone pair orbital contribution and the value of the normalized distance parameter, R_{XB}. This first ^{17}O NMR study on halogen bonding provides an interpretation of the correlation between the electronic structure of the halogen bond and ^{17}O NMR properties.

SSNMR studies of other σ-hole interactions, beyond the halogen bond, remain rare. Southern and Bryce recently reported a preliminary experimental and computational account of the impact of a carbon tetrel bond on the ^{13}C chemical shift of methyl groups in sarcosine and its

salts, as well as in various small model systems.[68] Such effects may prove to be useful in NMR crystallographic refinement protocols.

(iii) Structure Refinement

As described, NMR is a sensitive tool that can be used to probe the local chemical and electronic environment surrounding a nucleus of interest. NMR parameters can be extracted from the acquired spectra in order to characterize the local environment, which is supported by the analysis of X-ray diffraction and quantum chemical calculations. These calculations are an essential tool to NMR crystallographers, as they allow for the refinement of crystal structures by means of geometry optimization, which is of particular importance for hydrogen atoms. The results of geometry optimizations can subsequently be used to calculate the NMR parameters, as well as validate those which have been observed experimentally. When combined, experimental NMR data, quantum chemical calculations, and X-ray diffraction can lead to an accurate solution of the final crystal structure of a given compound.[48]

There is a significant body of literature focussed specifically on NMR crystallographic structure refinement.[2,69] Some examples were presented in the section on hydrogen bonding (*vide supra*). We present here only a few additional representative examples. For instance, Fernandes *et al*. fully characterized novel theophylline cocrystals (theophylline:4-aminobenzoic acid (1:1)) using NMR crystallography, and more importantly they provided information on internuclear proximities, especially hydrogen bonding, and the conformation of this compound by applying 1D/2D ^{1}H high-resolution solid-state NMR in the absence of a single-crystal X-ray structure.[70] Brouwer et al. have shown how large complexation-induced ^{1}H MAS SSNMR shifts of toluene and pyridine guests in *p-tert*-butylcalix[4]arene inclusion compounds can be

employed for NMR crystallography of host–guest complexes, providing important spatial information about the location of the guest molecules in the host cavities.[71]

Dynamic nuclear polarization (DNP) is a sensitivity increasing technique which transfers the polarization from the electrons to the nucleus, which has found its applications for NMR crystallography. Assignment of ^{13}C and ^{15}N resonances is sometimes hampered without the comparison of the experimental signals with the calculated chemical shifts, due to their low natural abundance, which can lead to uncertainties. Märker *et al*. overcame this problem of NMR by using MAS-DNP to record the 2D NMR of 2'-deoxy-3',5'-dipropanoylguanosine, a derivative of deoxyguanosine, at natural abundance.[72] A signal enhancement of >10 was observed allowing for spectral assignments to be carried out easily. Some examples of MAS-DNP experiments seen in this study that impact NMR crystallography are through space ^{13}C-^{13}C correlation experiments for long distance ^{13}C-^{13}C correlations, ^{13}C-^{13}C *J*-refocused INADEQUATE for one- and two-bonded correlations, and ^{15}N-^{13}C DCP-HETCOR for ^{15}N resonance assignment. Thanks to reduced dipolar truncation effects (typically observed for isotopically-enriched samples), DNP-enhanced solid-state NMR at natural isotopic abundance can be used as a new tool for NMR crystallography to measure long distances within structures.

NMR spectroscopy has the ability to provide information on several nuclei in inorganic materials. Sutrisno *et al.* applied solid-state multinuclear magnetic resonance to characterize zirconium phosphates and their derivatives. For Li-ZrP, Co-ZrP and ZrPOF-DEA, whose crystal structures were unknown, $^{6/7}Li$, ^{31}P, ^{13}C, and ^{19}F SSNMR spectra indicated the different crystallographic sites, giving partial structural information. The quadrupolar coupling constants and asymmetry parameters obtained from ^{91}Zr SSNMR show not only the distinct crystallographic sites, but also the distortion of Zr local environment upon ion exchange. For

other zirconium phosphates, whose crystal structures are known, in addition to structural information, the computational study of the magnitude of $C_Q(^{91}Zr)$ suggested that the geometric parameters around the Zr center, such as Zr-F and Zr-O bond distances as well as F-Zr-O and O-Zr-O bond angles, all contribute to the observed $C_Q(^{91}Zr)$ values.[73]

Brouwer and co-workers have implemented various approaches to refine or solve the structures of zeolites, silicates, and other network materials.[74,75,76] These innovative methods have yielded structure solutions in the absence of space group information, and also for noncrystalline materials where the information available from PXRD is limited. These methods rely on ^{29}Si-^{29}Si double-quantum NMR data to provide information on silicon-silicon connectivity, as well as two-bond ^{29}Si-^{29}Si *J* couplings when available. A recent example uses a simulated annealing approach to determine the structures of the pure silica zeolites ITQ-4, Ferrierite, and Sigma-2 from a two-dimensional ^{29}Si NMR correlation spectrum that probes nearest-neighbour interactions, combined with the unit cell parameters and space group information measured in a diffraction experiment.[76] This methodology convincingly demonstrates the value of combining the information available from NMR and PXRD to solve the structures of network materials.

As the vast majority of nuclides in the periodic table are quadrupolar, Perras and Bryce developed and applied a structure refinement protocol which uses EFG tensors measured using SSNMR spectroscopy and those calculated using the projector-augmented wave DFT method.[77] A least-squares optimization procedure was performed to minimize the difference between the experimental and the scaled calculated EFG tensors. This procedure yielded high-quality crystal structures comparable to those obtained from pure DFT energy minimizations, as judged by their root-mean-square deviations from single-crystal X-ray structures. Further improvement was

obtained by simultaneously refining the structures against the experimental EFG tensor parameters and optimizing the lattice energy with DFT. The methodology was demonstrated on $Na_2Al_2B_2O_7$, a member of an important family of nonlinear optical materials. The resulting structures were subjected to a systematic cross-validation process using experimental ^{23}Na, ^{11}B, ^{17}O, and ^{27}Al EFG and chemical shift data (Figure 6). A modified method was later applied to solve the structure of a zero thermal expansion material, $ZrMgMo_3O_{12}$, using ^{91}Zr, ^{25}Mg, ^{95}Mo, and ^{17}O MAS and high-resolution ^{17}O MQMAS NMR data, along with PXRD data.[78] The resulting structure was of sufficient detail that the observed zero thermal expansion could be explained using quantitative measures of the properties of the coordination polyhedra. It was also found that $ZrMgMo_3O_{12}$ shows significant ionic conductivity, a property that is also related to its structure.

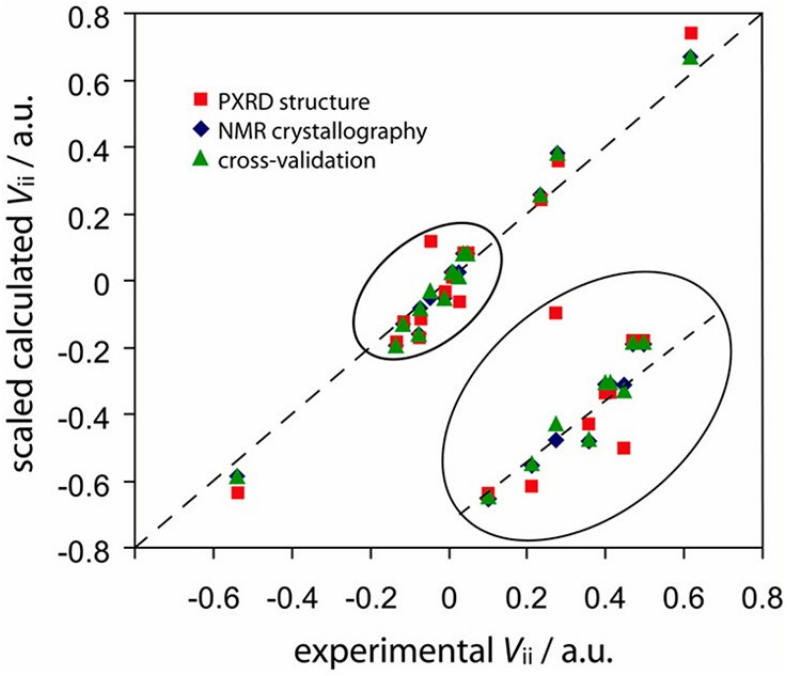

Figure 6. Comparison of the scaled calculated EFG tensor parameters from a PXRD structure (red squares), NMR crystallography (blue diamonds), and NMR cross-validation (green triangles) with those measured experimentally for all NMR-active isotopes in $Na_2Al_2B_2O_7$. Copyright American Chemical Society 2012. Used with permission. From reference 77.

(iv) Dynamics and Porous Materials

SSNMR is well-suited for the study of dynamic processes, as various NMR interactions and relaxation processes are sensitive to molecular motions. Such motion may be seen in pure compounds, and also in guest molecules which are encapsulated in host molecules. Porous materials such as metal-organic frameworks (MOFs) are frequently studied by SSNMR, not only to probe guest molecules, but also to probe the framework structures themselves, as these do not always crystallize with sufficient long-range order required for precise diffraction analyses.

Lu *et al.* showed clearly the crystallization process of 1D chain-like aluminophosphate **11** ($[AlP_2O_8H][N_2C_2H_{10}]$) and 3D open-framework aluminophosphates $AlPO_4$-12 ($[Al_3P_3O_{13}][N_2C_2H_{10}]$) by using ^{27}Al and ^{31}P MAS NMR throughout the solvothermal treatment period, which are heated in an autoclave loaded with the sample in the pre-heated oven (180℃) for 0, 0.5, 1, 2, 5, and 24 h (0, 1, 4, 6 ,12, and 72 h for $AlPO_4$-12).[79] Compound **11** has one crystallographically distinct four-coordinate Al atom (40.8 ppm) in the molecule. The intermediate Al sites during the crystallization at 44.8 ppm and -6.0 ppm were observed. ^{31}P MAS showed the two crystallographically distinct P sites (-10.5 and -12.4 ppm) in the final crystallized compound. During the crystallization process, the intermediate peaks (-6.6 and -14.0 ppm) were observed. Additional ^{31}P resonances (-15.6, -21.0, -23.5 ppm) are attributed to a possible solid-state product from reaction between excess polyphosphoric acid and unreacted Al source were highly resolved, which were not detectable in X-ray diffraction. ^{27}Al MAS NMR of $AlPO_4$-12 showed the change from the initial six-coordinated Al species to four- and five coordinated Al atoms. The final three crystallographically independent Al sites (two are from

the five–coordinated Al and one is four-coordinated Al) were resolved. The ^{31}P MAS NMR spectrum showed the presence of the long-range ordered salt of phosphoric acid and ethylenediamine initially, and the formation of aluminophosphate intermediates during the process. Finally, three crystallographically independent P sites were observed by diffraction in the structure of $AlPO_4$-12 and the signals obtained by ^{31}P MAS NMR could be attributed to these distinct phosphorus sites.

Huang and co-workers recently studied the paraelectric-ferroelectric phase transition of two isostructural MOFs, $[NH_4][M(HCOO)_3]$ (M=Mg, Zn), by applying in-situ variable-temperature ^{25}Mg, ^{67}Zn, ^{14}N and ^{13}C solid-state NMR.[80] A dramatic change in the ^{25}Mg SSNMR spectrum of $[NH_4][Mg(HCOO)_3]$ was observed upon lowering the temperature, with a loss of axial symmetry at magnesium noted between 243 and 233 K, as judged from the ^{25}Mg quadrupolar asymmetry parameter. A similar effect was observed via ^{67}Zn NMR in $[NH_4][Zn(HCOO)_3]$, where the transition occurred instead between 183 and 163 K. ^{14}N SSNMR experiments showed that the hydrogen bonding between NH_4^+ ions and framework oxygen atoms became stronger at lower temperature. Measurements of $C_Q(^{14}N)$ were used to demonstrate stronger hydrogen bonding in $[NH_4][Mg(HCOO)_3]$ as compared with $[NH_4][Zn(HCOO)_3]$ (Figure 7). Huang has also applied ^{13}C and ^{17}O SSNMR methodologies to deduce the nature of the motion of carbon dioxide molecules which are adsorbed in various MOFs.[81,82]

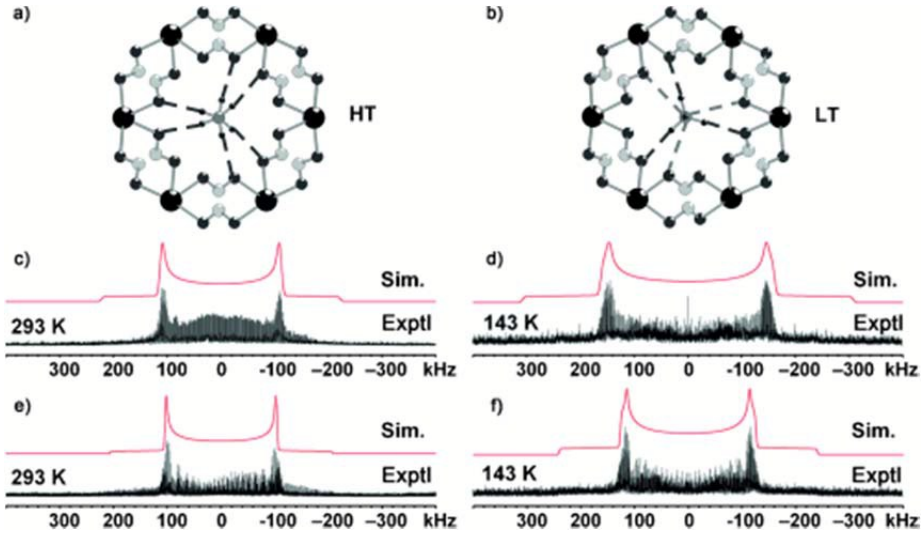

Figure 7. View down the channels of the Mg/Zn formate MOF in a) the HT paraelectric phase and b) the LT ferroelectric phase, as assembled from single-crystal XRD data. The H atoms of the formate ligands have been omitted for clarity. The hydrogen bonds between NH_4^+ and framework oxygen atoms in both structures are indicated by dashed lines. Experimental and simulated ^{14}N MAS NMR spectra of $[NH_4][Mg(HCOO)_3]$ at 293 K are shown in (c), with corresponding ^{14}N spectra of $[NH_4][Mg(HCOO)_3]$ at 143 K pictured in (d). The experimental and simulated ^{14}N NMR spectra of $[NH_4][Zn(HCOO)_3]$ at 293 K and 143 K are shown in e) and f), respectively. Copyright John Wiley and Sons, 2015. Used with permission. From reference 80.

Uchida *et al.* studied polymorphism of cubic cesium hydrogen silicododecatungstate crystals featuring mobile water molecules occupying vacancy sites.[83] ^{133}Cs MAS NMR indicated that in one preparation, CsHSiW-1, all the Cs^+ ions were in a homogenous environment surrounded by four Cs^+ ions and two polyoxometalate anions (POMs). In a second preparation, CsHSiW-3, the Cs^+ ions were found to be in three different environments due to anion vacancies. These were attributed to sites surrounded by 0, 1, and 2 POMs. By acquiring ^1H MAS solid-state NMR at 298 and 373 K, the state of water molecules inside the micropores has been investigated. In CsHSiW-1, there no signal was seen after heating to 373 K, implying the complete loss of water of crystallization, while at 298 K water was observed to be trapped in the intercrystallite space of the core, as indicated by a sharp signal at 5.6 ppm. For CsHSiW-3, a peak

corresponding to the water inside the intercrystallite space was observed after heating to 373 K. At 298 K, two peaks were observed: one for water inside the intercrystallite space (4.7 ppm), and one for water in the anion vacancies of the shell (4.2 ppm). Upon exposure of CsHSiW-3 to saturated water vapor, the peak at 4.2 ppm shifted towards 4.7 ppm, indicating that water could diffuse through the anion vacancies from the cell into the intercrystallite space of the core.

The clathrate hydrate lattice was engineered by adding NH_4F, and the resulting structures were explored using ^{129}Xe NMR as a probe of their void spaces.[84] Some water molecules were replaced with ammonium fluoride to prepare modified clathrate hydrate structures I and II. The ^{129}Xe MAS NMR results indicated that Structure I contained signals from Xe in both the large and small cages, whereas Structure II only had a peaks corresponding to Xe in the small cage. For both structures, with increasing initial NH_4F concentration, the xenon chemical shift values increase because of the decrease of the lattice constant and cage size. Information on the distribution of ions in the framework was also investigated. ^2H static NMR of methanol-d_4 was acquired at temperatures from 77 to 180 K to study the guest motion of methanol in the cage of Structure I. The stability of the modified methanol clathrate was attributed to strong methanol $CH_3OH\cdots F^-$ or $CH_3OH\cdots NH_4^+$ hydrogen bonding which leaves the water–water hydrogen bonding network intact, in contrast to the situation in a pure water clathrate where methanol–water hydrogen bonding disrupts the lattice and a stable clathrate cannot be made.

Yamada *et al.* have studied the dynamic behaviour of water clusters in the channels of 4-nitrostyrylpyridine hydrochloride by ^{17}O stationary SSNMR at temperatures ranging from 143 to 373 K.[85] The dynamics of water in the crystal may be classified into three phases based on the line shapes. In Phase I (from 143 to 273 K) water reoriented in the hydrophobic channel based on the activation energy was measured. Phase II (from 273 to 353 K) was an intermediate state

between ice and liquid water. Spectra of Phase III (above 353 K) showed an isotropic peak at 0 ppm, indicating an equilibrium of water molecules inside and outside the channel.

Potrzebowski has proposed a step by step methodology to refine peptide structures, demonstrated on the polymorphs of enkephalins (Tyr-Gly-Gly-Phe-Leu and Tyr-Gly-Gly-Phe-Met). This technique relied on the isotropic chemical shift, chemical shift tensor, and molecular dynamic analysis data.[86] First, they fully assigned all of the ^{13}C and ^{1}H resonances by applying ^{13}C and ^{1}H 1D SSNMR as well as ^{1}H-^{13}C and ^{1}H-^{15}N 2D inverse HETCOR MAS 2D NMR correlations for all three models. The values of the principal components of the ^{13}C CSA tensors, δ_{ii}, were obtained by separating the spinning sidebands of each nucleus through 2D PASS.[87] The molecular motion was analyzed by comparing the calculated dipolar coupling constant and the experimentally measured splitting using 2D PISEMA MAS. This indicated the presence of at least two distinct molecular motions in the asymmetric unit. By comparing the correlations between the experimental and computed ^{13}C chemical shift principal components using the coordinates from the crystallographic database and the optimized coordinates of the heavy atoms and protons, more reasonable coordinates that better correlate to the real samples were generated to provide fine refinements of the crystal structures.

Deuterium SSNMR is a classic method for probing molecular dynamics in solids.[5,16,88] ^{2}H is a spin-1 nuclide and has a small nuclear quadrupole moment, which typically leads to quadrupolar coupling constants up to several hundred kHz. Slow, intermediate, and fast motion regimes, compared to the quadrupolar frequency, may be probed by observing a reduction in the value of C_Q expected in the absence of motion. By recording deuterium solid-state NMR spectra over a range of temperatures, the spectra may be modelled to extract detailed information on molecular dynamics, including both the rate and the nature of the motion. For example,

Frischmann et al. investigated the dynamics of *N*, *N*-dimethylformamide (DMF) encapsulated within cadmium metallocavitands with solid-state ^{2}H NMR spectroscopy, demonstrating 3-fold rotation of the guest with an activation energy of 14.4 ± 1 kJ mol^{-1} (see Figure 8).[89] Schurko, Loeb, and co-workers have published an important series of articles which detail deuterium SSNMR studies of MOF materials featuring dynamic interlocked components.[90,91,92] In a related example, the motion of molecular shuttling of a macrocyclic ring along a rigid strut of a zinc-based MOF was examined variable-temperature ^{1}H-^{13}C cross-polarization/magic-angle spinning (CP/MAS) and ^{13}C 2D exchange correlation spectroscopy (EXSY) solid-state NMR.[93] Garcia-Garibay and co-workers have also published several beautiful examples demonstrating the value of SSNMR methods in probing molecular dynamics in engineered molecular rotors.[94,95.96,97,98]

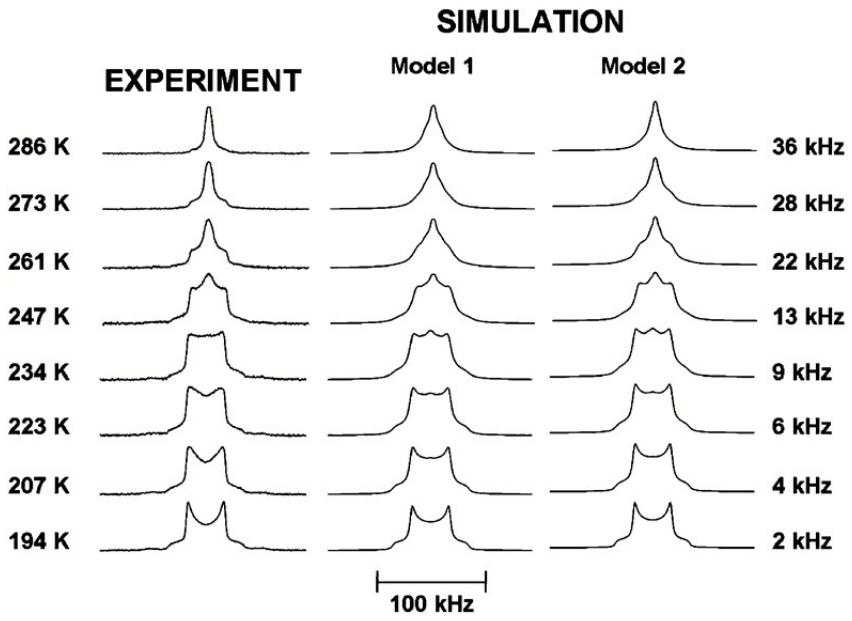

Figure 8. Experimental and simulated solid-state ^{2}H NMR spectra for DMF-d_7 trapped in the capsules of a cadmium cluster metallocavitand measured as a function of temperature. Model 1 is a 3-fold rotation of the N-$(CD_3)_2$ moiety about the bisector of the (CD_3)−N−(CD_3) bond angle. Model 2 is an overall three-fold molecular rotation about an axis defined by DFT calculations. Copyright American Chemical Society 2010. Used with permission. From reference 89.

It may be a challenge for X-ray diffraction to analyze guests embedded inside porous matrices since X-ray beams are diffracted from the surface of the material. Yang *et al*. confirmed that in this context solid-state NMR offers a distinctive advantage.[99] They analyzed the crystallinity and crystalline forms of four different organic compounds: ibuprofen, fenofibrate, griseofulvin, and indomethacin after crystallization in porous materials by ^{13}C CP/MAS. They were able to quantitatively measure the ratio of two polymorphs by measuring the integration ratio of two peaks in the spectra of ibuprofen. Comparison between the ^{13}C CP/MAS spectra of griseofulvin before and after strong washing with cold solvent indicated that polymorph II and amorphous material formed inside the silica pore could be maintained.

Concluding Remarks

This article, by its very nature, has only provided selected snapshots of the intersection of the fields of solid-state NMR spectroscopy and crystal engineering. Broadly speaking, the role of SSNMR in crystal engineering is two-fold. Firstly, a wide range of SSNMR methodologies may be brought to bear on the chemical and/or crystallographic identity and structure of an engineered material. The depth of this analysis ranges from simple fingerprinting to a full structure solution, often in concert with diffraction and computational data. This procedure may provide *de novo* information, or in other instances it may be used in a confirmatory capacity; this is analogous to the current practices for solution NMR and powder XRD, for example. Secondly, NMR can provide direct insight into fine details associated with the properties and potential functions of engineered materials. These include, for example, the dynamics of molecular rotors and motors, the detailed atomic arrangement (including protons) about intra-

and intermolecular non-covalent bonds, and adsorption properties of porous materials. This information is useful in and of itself, but also has significant value in the iterative cycle of crystal engineering, whereby new materials are designed and constructed on the basis of what has been learnt from the previous iterations.

Acknowledgements

D. L. B. is grateful to the Natural Sciences and Engineering Research Council of Canada for funding.

Author Biographies

Yijue Xu graduated from the University of Ottawa (Ottawa, Ontario) with a B. Sc. (Hons.) degree with specialization in biochemistry in 2015. Her honours thesis was on the characterization of halogen-bonded solids by ^{31}P and ^{17}O solid-state multinuclear magnetic resonance under the supervision of Professor David Bryce. She is currently a Masters student in the Department of Chemistry and Biomolecular Sciences and is studying halogen bonding interactions via single-crystal NMR as well as real-time NMR studies of mechanochemical reactions.

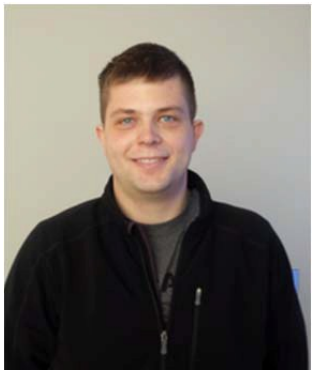

Scott A. Southern is a Ph.D. candidate in Chemistry at the University of Ottawa. After earning both a B. Sc. (Hons) in Biochemistry as well as Biopharmaceutical Sciences at the University of Ottawa, he began his graduate studies under the supervision of David L. Bryce. Over this period,

during which time he earned a M.Sc. degree, his research interests have included the solid-state NMR analysis carbon and lead tetrel bonds by solid-state NMR. He has also worked on the quantum chemical analysis of NMR parameters related to metal-metal bonding in solids.

Patrick M.J. Szell is a Ph.D. student in the group of David L. Bryce at the University of Ottawa. He earned his B. Sc. (Hons) in Biomedical Sciences from the University of Ottawa in 2014. His research is focused on the study of halogen bonding using multinuclear solid-state NMR and X-ray diffraction.

David L. Bryce is currently Full Professor and University Research Chair in Nuclear Magnetic Resonance at the University of Ottawa. He earned his B. Sc. (Hons) in Chemistry from Queen's

University (Kingston, Ontario) in 1998, followed by a Ph.D. in 2002 from Dalhousie University (Halifax, Nova Scotia), where he worked with Rod Wasylishen. Following postdoctoral work at the Laboratory of Chemical Physics (National Institutes of Health, Bethesda, Maryland) with Ad Bax, he took up a faculty position in his home city of Ottawa in 2005. Current research interests include solid-state NMR of low-frequency quadrupolar nuclei, NMR studies of materials, quantum chemical interpretation of NMR interaction tensors, and halogen bonding. He currently serves as Trends Editor for *Solid State Nuclear Magnetic Resonance* and as the Section Editor for Magnetic Resonance and Molecular Spectroscopy for the *Canadian Journal of Chemistry*.

References

[1] http://www.rsc.org/journals-books-databases/about-journals/crystengcomm/

[2] *NMR Crystallography*, ed. R. K. Harris; R. E. Wasylishen; M. J. Duer, John Wiley and Sons Ltd.: Chichester, U. K., 2009.

[3] G. R. Desiraju. *J. Am. Chem. Soc.*, 2013, **135**, 9952-9967.

[4] M. J. Duer. *Introduction to Solid-State NMR Spectroscopy*. Wiley-Blackwell, Malden, 2005.

[5] D. L. Bryce, G. M. Bernard, M. Gee, M. D. Lumsden, K. Eichele, R. E. Wasylishen, *Can. J. Anal. Sci. Spectrosc.* 2001, **46**, 46-82.

[6] F. Taulelle, *Solid State Sci.* 2004, **6**, 1053-1057.

[7] M. R. Chierotti, R. Gobetto, *CrystEngComm,* 2013, **15**, 8599-8612.

[8] J. Vaara, J. Jokisaari, R. E. Wasylishen, D. L. Bryce, *Prog. Nucl. Magn. Reson. Spectrosc.* 2002, **41**, 233-304.

[9] P. S. Camacho, K. S. A. Arachchige, A. M. Z. Slawin, T. F. G. Green, J. R. Yates, D. M. Dawson, J. D. Woollins, S. E. Ashbrook, *J. Am. Chem. Soc.* 2015, **137**, 6172-6175.

[10] F. R. Knight, L. M. Diamond, K. S. A. Arachchige, P. S. Camacho, R. A. M. Randall, S. E. Ashbrook, M. Bühl, A. M. Z. Slawin, J. D. Woollins, *Chem. Eur. J.* 2015, **21**, 3613-3627.

[11] F. A. Perras, D. L. Bryce, *J. Am. Chem. Soc.* 2013, **135**, 12596-12599.

[12] F. A. Perras, D. L. Bryce, *J. Phys. Chem. Lett.* 2014, **5**, 4049-4054.

[13] F. A. Perras, D. L. Bryce, *eMagRes* 2015, **4**, 561-574.

[14] C. M. Widdifield, D. L. Bryce, *Phys. Chem. Chem. Phys.* 2009, **11**, 7120-7122.

[15] C. M. Widdifield, F. A. Perras, D. L. Bryce, *Phys. Chem. Chem. Phys.* 2015, **17**, 10118-10134.

[16] K. Schmidt-Rohr and H. W. Spiess, Multidimensional Solid-State NMR and Polymers, Academic Press, London, 1994.

[17] D. C. Apperley, R. K. Harris, P. Hodgkinson, Solid State NMR Basic Principles & Practice. Momentum Press, New York, 2012.

[18] M. A. Kennedy, P. D. Ellis, *Concepts in Magn. Reson.*, 1989, **1**, 35; *ibid.* 1989, **1**, 109.

[19] S. J. Opella, *Acc. Chem. Res.* 2013, **46**, 2145-2153.

[20] W. T. Dixon, J. Schaefer, M. D. Sefcik, E. O. Stejskal, R. A. McKay, *J. Magn. Reson.* 1982, **49**, 341-345.

[21] D. Sakellariou, A. Lesage, P. Hodgkinson, L. Emsley, *Chem. Phys. Lett.* 2000, **319**, 253-260.

[22] J.-P. Amoureux, M. Pruski, *eMagRes*, 2007. DOI: 10.1002/9780470034590.emrstm0319.pub2

[23] Y. Wu, *eMagRes*, 2007. DOI: 10.1002/9780470034590.emrstm0135

[24] P. J. Grandinetti, *eMagRes*, 2011. DOI: 10.1002/9780470034590.emrstm0137.pub2

[25] Z. Gan, *eMagRes*, 2007. DOI: 10.1002/9780470034590.emrstm0481

[26] J.-D. Mao, W.-G. Hu, K. Schmidt-Rohr, G. Davies, E. A. Ghabbour, B. Xing, *Soil Sci. Soc. Am. J.* 2000, **64**, 873-884.

[27] J. R. Patel, R. A. Carlton, F. Yuniatine, T. E. Needham, L. Wu, F. G. Vogt, *J. Pharm. Sci.* 2012, **101**, 641-663.

[28] W. Cai, R. D. Piner, F. J. Stadermann, S. Park, M. A. Shaibat, Y. Ishii, D. Yang, A. Velamakanni, S. J. An, M. Stoller, J. An, D. Chen, R. S. Ruoff, *Science*, 2008, **321**, 1815-1817.

[29] D. Bardelang, A. Brinkmann, C. I. Ratcliffe, J. A. Ripmeester, V. V. Terskikh, K. A. Udachin, *CrystEngComm*, 2014, **16**, 3788-3795.

[30] M. Schmidt, C. S. Zehe, R. Siegel, J. U. Heigl, C. Steinlein,H.-W. Schmidt, J. Senker, *CrystEngComm*, 2013, **15**, 8784-8796.

[31] J. Bernstein, *Polymorphism in Molecular Crystals*, Oxford University Press, New York, 2007.

[32] S. R. Chemburkar, J. Bauer, K. Deming, H. Spiwek, K. Patel, J. Morris, R. Henry, S. Spanton, W. Dziki, W. Porter, J. Quick, P. Bauer, J. Donaubauer, B. A. Narayanan, M. Soldani, D. Riley and K. McFarland, *Org. Process Res. Dev.* 2000, **4**, 413–417.

[33] G. D. Enright, V. V. Terskikh, D. H. Brouwer, J. A. Ripmeester, *Cryst. Growth Des.* 2007, **7**, 1406-1410.

[34] S. L. Veinberg, Z. W. Friedl, K. J. Harris, L. A. O'Dell, R. W. Schurko, *CrystEngComm.* 2015, **17**, 5225-5236.

[35] M. Hildebrand, H. Hamaed, A. M. Namespectra, J. M. Donohue, R. Fu, I. Hung, Z. Gan, R. W. Schurko, *CrystEngComm.* 2014, **16**, 7334-7356.

[36] K. M. N. Burgess, D. L. Bryce, *Solid State Nucl. Magn. Reson*. 2015, **65**, 75-83.

[37] L. Wang, M. Luo, J. Li, J. Wang, H. Zhang, Z. Deng, *Cryst. Growth Des.* 2015, **15**, 2574-2578.

[38] M. M. H. Smets, S. J. T. Brugman, E. R. H. van Eck, J. A. van den Ende, H. Meekes, H. M. Cuppen, *Cryst. Growth Des.* 2015, **15**, 5157-5167.

[39] T. Pawlak, P. Paluch, K. Trzeciak-Karlikowska, A. Jeziorna, M. J. Potrzebowski, *CrystEngComm*, 2013, **15**, 8680-8692.

[40] K. M. N. Burgess, F. A. Perras, A. Lebrun, E. Messner-Henning, I. Korobkov; D. L. Bryce, *J. Pharm. Sci.* 2012, **101**, 2930-2940.

[41] A. D. Bond, C. Cornett, F. H. Larsen, H. Qu, D. Raijada, J. Rantanen, *Cryst. Growth Des.* 2013, **13**, 3665-3671.

[42] D. C. Apperley, A. F. Markwell, R. K. Harris, P. Hodgkinson, *Magn. Reson. Chem.* 2012, **50**, 680-690.

[43] R. K. Chandrappa, P. Ochsenbein, C. Martineau, M. Bonin, G. Althoff, F. Engelke, H. Malandrini, B. Castro, M. E. Hajji and F. Taulelle, *Cryst. Growth Des.* 2013, **13**, 4678–4687.

[44] E. Halevas, A. Hatzidimitriou, M. Bertmer, A. A. Vangelis, A. Antzara, C. Mateescu, A. Salifoglou, *Cryst. Growth Des.* 2014, **14**, 4041-4059.

[45] B. A. Hammann, Z. L. Ma, K. M. Wentz, M. K. Kamunde-Devonish, D. W. Johnson, S. E. Hayes, *Dalton Trans.*, 2015, **44**, 17652-17659.

[46] J. S. Murray, P. Lane, P. Politzer, *J. Mol. Model.* 2009, **15**, 723-729.

[47] A. S. Tatton, T. N. Pham, F. G. Vogt, D. Iuga, A. J. Edwards, S. P. Brown, *Mol. Pharmaceutics* 2013, **10**, 999-1007.

[48] A. L. Webber, L. Emsley, R. M. Claramunt, S. P. Brown, *J. Phys. Chem. A.* 2010, **114**, 10435-10442.

[49] J. P. Bradley, S. P. Velaga, O. N. Antzutkin, S. P. Brown, *Cryst. Growth Des.* 2011, **11**, 3463-3471.

[50] K. Pogorzelec-Glaser, A. Rachocki, P. Lawniczak, A. Pietraszko, C. Pawlaczyk, B. Hilczer, M. Pugaczowa-Michalska, *CrystEngComm*, 2013, **15**, 1950-1959.

[51] A. Rachocki, K. Pogorzelec-Glaser, P. Lawniczak, M. Pugaczowa-Michalska, A. Łapiński, B. Hilczer, M. Matczak, A. Pietraszko, *Cryst. Growth Des.* 2014, **14**, 1211-1220.

[52] G. J. Rees, S. P. Day, A. Lari, A. P. Howes, D. Iuga, M. B. Pitak, S. J. Coles, T. L. Threlfall, M. E. Light, M. E. Smith, D. Quigley, J. D. Wallis, J. V. Hanna, *CrystEngComm*, 2013, **15**, 8823-8839.

[53] A. Wong, K. J. Pike, R. Jenkins, G. J. Clarkson, T. Anupold, A. P. Howes, D. H. G. Crout, A. Samoson, R. Dupree, M. E. Smith, *J. Phys. Chem. A* **2006**, 110, 1824-1835

[54] F. G. Vogt, H. Yin, R. G. Forcino, L. Wu, *Mol. Pharmaceutics*, 2013, **10**, 3433-3446.

[55] D. Braga, L. Chelazzi, F. Grepioni, E. Dichiarante, M. R. Chierotti, R. Gobetto, *Cryst. Growth Des.* 2013, **13**, 2564-2572.

[56] D. L. Bryce, M. Gee, R. E. Wasylishen, *J. Phys. Chem. A* 2001, **105**, 10413-10421.

[57] D. L. Bryce, G. D. Sward, S. Adiga, *J. Am. Chem. Soc.* 2006, **128**, 2121-2134.

[58] M. Sardo, S. M. Santos, A. A. Babaryk, C. López, I. Alkorta, J. Elguero, R. M. Claramunt, L. Mafra, *Solid State Nucl. Magn. Reson.* 2015, **65**, 49-63.

[59] J. Xu; V. V. Terskikh; Y. Chu; A. Zheng; Y. Huang, *Chem. Mater.* 2015, **27**, 3306-3316.

[60] G. Cavallo, P. Metrangolo, R. Milani, T. Pilati, A. Priimagi, G. Resnati, G. Terraneo, *Chem. Rev.* 2016, **116**, 2478-2601.

[61] D. L. Bryce and J. Viger-Gravel, *Top. Curr. Chem.* 2015, **358**, 183-204.

[62] C. M. Widdifield, G. Cavallo, G. A. Facey, T. Pilati, J. Lin, P. Metrangolo, G. Resnati, D. L. Bryce, *Chem. Eur. J.* 2013, **19**, 11949-11962.

[63] R. J. Attrell, C. M. Widdifield, I. Korobkov, D. L. Bryce, *Cryst. Growth Des.* 2012, **12**, 1641-1653.

[64] J. Viger-Gravel, S. Leclerc, I. Korobkov, D. L. Bryce, *CrystEngComm.* 2013, **15**, 3168-3177.

[65] J. Viger-Gravel, S. Leclerc, I. Korobkov, D. L. Bryce, *J. Am. Chem. Soc.* 2014, **136**, 6929-6942.

[66] J. Viger-Gravel, J. E. Meyer, I. Korobkov, D. L. Bryce, *CrystEngComm,* 2014, **16**, 7285-7297.

[67] Y. Xu, J. Viger-Gravel, I. Korobkov, D. L. Bryce, *J. Phys. Chem. C* 2015, **119**, 27104-27117.

[68] S. A. Southern, D. L. Bryce, *J. Phys. Chem. A* 2015, **119**, 11891-11899.

[69] S. E. Ashbrook, D. McKay, *Chem. Commun.* 2016, DOI: 10.1039/c6cc02542k

[70] J. A. Fernades, M. Sardo, L. Mafra, D. Choquesillo-Lazarte, N. Masciocchi, *Cryst. Growth Des.* 2015, **15**, 3674-3683.

[71] D. H. Brouwer, S. Alavi, J. A. Ripmeester, *Phys. Chem. Chem. Phys.* 2008, **10**, 3857-3860.

[72] K. Märker, M. Pingret, J.-M. Mouesca, D. Gasparutto, S. Hediger, G. D. Paëpe, *J. Am. Chem. Soc.* 2015, **137**, 13796-13799.

[73] A. Sutrisno, L. Liu, J. Dong, Y. Huang, *J. Phys. Chem. C* 2012, **116**, 17070-17081.

[74] D. H. Brouwer, S. Cadars, J. Eckert, Z. Liu, O. Terasaki, B. F. Chmelka, *J. Am. Chem. Soc.* 2013, **135**, 5641-5655.

[75] D. H. Brouwer, *Solid State Nucl. Magn. Reson.* 2013, **51-52**, 37-45.

[76] D. H. Brouwer, M. Horvath, *Solid State Nucl. Magn. Reson.* 2015, **65**, 89-98.

[77] F. A. Perras, D. L. Bryce, *J. Phys. Chem. C* 2012, **116**, 19472-19482.

[78] C. P. Romao, F. A. Perras, U. Werner-Zwanziger, J. A. Lussier, K. J. Miller, C. M. Calahoo, J. W. Zwanziger, M. Bieringer, B. A. Marinkovic, D. L. Bryce, M. A. White, *Chem. Mater.* 2015, **27**, 2633-2646.

[79] H. Lu, J. Xu, P. Gao, W. Yan, F. Deng, R. Xu, *Microporous and Mesoporous Materials* 2015, **208**, 105-112.

[80] J. Xu, B. E. G. Lucier, R. Sinelnikov, V. V. Terskikh, V. N. Staroverov, Y. Huang, *Chem. Eur. J.* 2015, **21**, 14348-14361.

[81] W. D. Wang, B. E. G. Lucier, V. V. Terskikh, W. Wang, Y. Huang, *J. Phys. Chem. Lett.* 2014, **5**, 3360-3365.

[82] Y. Zhang, B. E. G. Lucier, Y. Huang, *Phys. Chem. Chem. Phys.* 2016, **18**, 8327-8341.

[83] S. Uchida, Y. Ogasawara, T. Maruichi, A. Kumamoto, Y. Ikuhara, T. Yamada, H. Kitagawa, N. Mizuno, *Cryst. Growth Des.* 2014, **14**, 6620-6626.

[84] K. Shin, I. L. Moudrakovski, M. D. Davari, S. Alavi, C. I. Ratcliffe, J. A. Ripmeester, *CrystEngComm*, 2014, **16**, 7209-7217.

[85] S. Yamada, N. Sako, K. Yamada, K. Deguchi, T. Shimizu, *CrystEngComm*. 2015, **17**, 5629-5633.

[86] T. Pawlak, M. J. Potrzebowski, *J. Phys. Chem. B* 2014, **118**, 3298-3309.

[87] O. N. Antzutkin, S. C. Shekar, M. H. Levitt, *J. Magn. Reson., Ser. A* 1995, **115**, 7−19.

[88] R. J. Wittebort, E. T. Olejniczak, R. G. Griffin, *J. Chem. Phys.* 1987, **86**, 5411–5420.

[89] P. D. Frischmann, G. A. Facey, P. Ghi, A. J. Gallant, D. L. Bryce, F. Lelj, and M. J. MacLachlan, *J. Am. Chem. Soc.* 2010, **132**, 3893–3908.

[90] V. N. Vukotic, C, A. O'Keefe, K. Zhu, K. J. Harris, C. To, R. W. Schurko, S. J. Loeb, *J. Am. Chem. Soc.* 2015, **137**, 9643–9651.

[91] K. Zhu, V. N. Vukotic, C. A. O'Keefe, R. W. Schurko, S. J. Loeb, *J. Am. Chem. Soc.* 2014, **136**, 7403−7409.

[92] V. N. Vukotic, K. J. Harris, K. Zhu, R. W. Schurko, S. J. Loeb, *Nature Chem.* 2012, **4**, 456-460.

[93] K. Zhu, C. A. O'Keefe, V. N. Vukotic, R. W. Schurko, S. J. Loeb, *Nature Chem.* 2015, **7**, 514-519.

[94] X. Jiang, B. Rodriguez-Molina, N. Nazarian, M. A. Garcia-Garibay, *J. Am. Chem. Soc.* 2014, **136**, 8871-8874.

[95] S. Pérez-Estrada, B. Rodríguez-Molina, L. Xiao, R. Santillan, G. Jiménez-Osés, K. N. Houk, M. A. Garcia-Garibay, *J. Am. Chem. Soc.* 2015, **137**, 2175-2178.

[96] L. Catalano, S. Pérez-Estrada, G. Terraneo, T. Pilati, G. Resnati, P. Metrangolo, M. A. Garcia-Garibay, *J. Am. Chem. Soc.* 2015, **137**, 15386-15389.

[97] D. Czajkowska-Szczykowska, A. Aguilar-Granda, J. Maj, A. Z. Wilczewska, S. Witkowski, R. Santillan, M. A. Garcia-Garibay, J. W. Morzycki, B. Rodríguez-Molina, *Cryst. Growth Des.* 2016, **16**, 1599-1605.

[98] X. Jiang, Z. J. O'Brien, S. Yang, L. H. Lai, J. Buenaflor, C. Tan, S. Khan, K. N. Houk, M. A. Garcia-Garibay, *J. Am. Chem. Soc.* 2016, **138**, 4650-4656.

[99] X. Yang, T. C. Ong, V. K. Michaelis, S. Heng, J. Huang, R. G. Griffin, A. S. Myerson, *CrystEngComm*, 2014, **16**, 9345-9352.